

Embedded Wireless Sensor Design for Long Term Structural Health Monitoring

Christopher Bessin², Patrick Blum¹, Matthew P. Iannucci¹, Jordan T. Kirby¹, Zachary McIntosh¹, Elizabeth L. Paul², Michael A. Regan¹, Justin W. Skenyon², Charles J. Wesley¹, and Samuel D. Wiley¹

¹Finite Element Modelling

²Instrumentation Development

May 14, 2014

Abstract

Structural Health Monitoring(SHM) is the process of evaluating and assessing fatigue of existing infrastructure by continuously monitoring long term changes in natural frequency vibration. Aging traffic infrastructure is a growing problem across the world as material and construction cost has risen considerably in recent decades. As replacement becomes more difficult reliable lifetime extension is possible through structural health monitoring. At the completion of this project a sensor package was designed and partially assembled, a simple finite element model (FEM) of the main span was produced, high precision GPS units were installed and collected data for two weeks, and preliminary data was collected with the package accelerometers on top of the towers of the bridge. With development and research damage location, type, and severity may be indicated by interpreting the vibration changes.

Contents

1	Introduction	7
1.1	Objectives	7
1.1.1	Phase One (Fall 2013)	7
1.1.2	Phase Two (Spring 2014)	7
1.2	Layout	7
2	Finite Element Model (FEM)	9
2.1	Introduction	9
2.1.1	Background of the Claiborne Pell Bridge	9
2.1.2	Introduction to FEM	9
2.2	Abaqus FEM Verification	10
2.2.1	L Beam Analysis	10
2.3	Claiborne Pell Bridge Model	11
2.3.1	Modeling Large Suspension Bridges	11
2.3.2	Modeling Process	11
2.3.3	Limitations of Abaqus Model	13
3	Instrumentation Package	15
3.1	Introduction	15
3.2	Introduction	15
3.3	Microprocessor	15
3.3.1	Necessary Specifications	16
3.3.2	Platform Options	17
3.3.3	Platform Decision	18
3.4	Sensors	18
3.4.1	Accelerometer	18
3.4.2	Strain Gauge	21
3.4.3	Strain Gauge Selection	23
3.4.4	GPS Receiver	25
3.4.5	Analog to Digital Converter	26
3.5	Electrical Design	30
3.5.1	Introduction	30
3.5.2	Circuitry	30
3.5.3	Printed Circuit Board	31
3.6	Software Design	32

3.7	Package Power	34
3.7.1	Power Budget	34
3.7.2	Package Power	35
3.7.3	Wind Potential	39
3.8	Battery Selection	45
4	Data Collection	47
4.1	Phase One Data Collection	47
4.1.1	6g Tri-Axial Accelerometer Data	47
4.2	Phase Two Data Collection	47
4.2.1	6g Tri-Axial Accelerometer Data	47
4.2.2	Cell Phone Accelerometer	48
4.2.3	Battery Discharge	50
4.2.4	Solar Panels	50
4.2.5	Wind Turbine	50
5	Data Analysis	54
5.1	Phase One Data Analysis	54
5.1.1	Comparison of Preliminary Abaqus Model and Preliminary Data	54
5.2	Phase Two Data Analysis	55
5.2.1	Comparison of Developed Abaqus Model with Literature	55
6	Future Development	57
6.1	Instrumentation	57
6.1.1	Integration of Strain Gauge	57
6.1.2	Wireless Transmission	57
6.1.3	GPS Time Synchronization	58
6.1.4	Package Assembly	59
6.2	Package Enclosure	60
6.3	Package Location	66
6.4	FEM	67
6.4.1	Model Improvements	67
6.4.2	Dynamic Loading	68
7	Conclusion	70
A	Sensor Package Schematics	73
A.1	LM317 Adjustable Voltage Regulators	73
A.2	BeagleBone Black	74
A.3	MMA7361 Accelerometer	75
A.4	MCP606 Op-Amp Buffer Circuit	76
A.5	ADS1113 Analog-Digital Converter	77
A.6	Trimble Copernicus II GPS Receiver	78
B	Enclosure Options	79

C Battery Log	81
C.1 Battery Log	81

List of Figures

3.1	<i>3-Element Rosette, metal-foil type strain gauge Manufacturer: Omega</i>	22
3.2	<i>Wheatstone Bridge Circuit Schematic[6]</i>	23
3.3	<i>Graph showing the relationship between gauge factor and temperature change[6]</i>	24
3.4	<i>Omega 3-Element Rosette with leads attached</i>	24
3.5	<i>Copernicus II GPS receiver</i>	26
3.6	<i>GPS sentence data and PPS signal recorded with oscilloscope for preliminary analysis.</i>	26
3.7	<i>Chart displaying the classifications of different ADC architectures [14]</i>	27
3.8	<i>Standard configuration of op-amp as a buffer</i>	31
3.9	<i>Software flow of the sensor package</i>	34
3.10	<i>Newport Radiation - 20 years</i>	36
3.11	<i>Newport Radiation</i>	36
3.12	<i>SolarPanel</i>	38
3.13	<i>2012 NOAA Wind Data at 6.4 meters</i>	40
3.14	<i>Computed 2012 NOAA Wind Data at 50 meters</i>	41
3.15	<i>Probability Density Graph of Computed Data</i>	42
3.16	<i>Hourly watt output</i>	43
3.17	<i>Cumulative power</i>	44
3.18	<i>Mass and Volume Energy Densities for Various Battery Chemistries</i>	46
4.1	<i>FFT of 6g data</i>	48
4.2	<i>Location comparison</i>	49
4.3	<i>Discharge of batteries with 2 loads</i>	51
4.4	<i>Current output of 5W solar panel</i>	52
4.5	<i>Voltage output from turbine</i>	53
5.1	<i>Modal Response of Abaqus Model</i>	56
6.1	<i>Omega 3-Element Rosette with pre-soldered leads.</i>	58
6.2	<i>Example Mating Mechanisms</i>	62
6.3	<i>USB 2.0A External Connector (LTWUA-20AMFM-SL7A) from Ampehnol LTW</i>	62
6.4	<i>Shielded Ethernet External Connector (RJ45-5EWTP-QR-PCB) from Video Production Inc</i>	63
6.5	<i>Cable Gland (CB-GD-5000045) from AA Power Corp</i>	63

6.6	<i>MCX Jack-to-Jack Adapter (252171) from Aamphenol Connex with Size Reference</i>	64
6.7	<i>Waterproof SMA Bulkhead Connector (9153-7553-002) from Applied Engineering Products with Size Reference</i>	64
6.8	<i>Potential Layout of a Pelican 1400 Model Case. The red arrows depict a 12V power supply, the yellow arrows depict a 3.3V power supply, and the green arrows depict the transfer of communications.</i>	65
6.9	<i>Neodymium Mounting Magnet</i>	66
6.10	<i>Proposed Package Mounting Location</i>	67
6.11	<i>Proposed Location for Sensor Package, Wind Turbine and Solar Panels</i>	69
A.1	<i>Schematic of 5V and 3.3V voltage regulator circuit</i>	73
A.2	<i>Schematic of BeagleBone Black</i>	74
A.3	<i>Schematic of MMA7361 $\pm 1.5g / \pm 6g$ Tri-Axial Accelerometer</i>	75
A.4	<i>Schematic of MCP606 ADC Input Buffer Circuit</i>	76
A.5	<i>Schematic of four ADS1113 ADC units in parallel</i>	77
A.6	<i>Schematic of Copernicus II GPS Receiver</i>	78

List of Tables

2.1	<i>Comparison between Abaqus models</i>	11
3.1	<i>Comparison table of two microprocessors that were looked into for the embedded sensor package</i>	17
3.2	<i>Comparison table of four accelerometers that were possible candidates for the sensor package.</i>	20
3.3	<i>Comparison table of the ADS1211, ADS1115 and ADS1113 ADC devices</i>	28
3.4	<i>LM317 Adjustable Linear Regulator Specifications</i>	30
3.5	<i>Time without power production</i>	35
3.6	<i>Time without power production</i>	43
5.1	<i>Comparison between analytical, model and experimental results</i>	54
5.2	<i>Comparison between analytical and experimental results</i>	55
5.3	<i>First five modes comparison for Abaqus and Journal Article</i>	55
B.1	<i>Brief summary of enclosure options considered for the sensor package</i>	80

Chapter 1

Introduction

1.1 Objectives

1.1.1 Phase One (Fall 2013)

Verify Abaqus software as a viable software package for future modeling by comparing the natural frequencies for a simply supported beam produced by a computed model with the analytical solution. Design and assemble a sensor package capable of accurately collecting vibration data. Collect data from the simply supported beam that concurs with results from analytical solution and model. This package was missing three main components; power independence, wireless communication capabilities, and GPS time synchronization.

1.1.2 Phase Two (Spring 2014)

Produce a FEM of the Claiborne Pell Bridge to identify locations for sensor packages installation based on modal response and to indicate the approximate natural frequencies to expect from bridge. Complete sensor packages, install them on the bridge in specified locations, and transmit data for frequency evaluation.

1.2 Layout

This report will discuss the planning process of designing a sensor package intended to evaluate vibration on the Claiborne Pell Bridge. As this is a two-semester project the preliminary assembly of the package was simplified to evaluate vibrations of a 6.8 meter angle beam in phase one. A finite element model was produced of this angle beam to provide information on the modes of vibration and natural frequency. In the second semester the package was further developed but not completed. Data was collected from the top of the towers by a prototype package. A FEM was produced of the Claiborne Bridge and used to evaluate approximate natural frequencies of the bridge and to indicate where the package should be

installed for best results.

Chapter 2 explains the process of the finite element model that was produced for both the angle beam and the Claiborne Bridge. The specific parameters used to describe the material are described in detail. To prove that the finite element model was reflecting accurate natural frequencies and modes of vibration, the model for the angle beam was verified with an analytical solution.

Choosing appropriate cooperating instrumentation is critical to producing a sensor package that will accurately monitor vibration frequencies. Chapter 3 of this report will present the instrumentation chosen and why.

Three separate data sets were recorded; that of the angle beam, the bridge, and the battery discharge curve. The collection process and processing details are discussed in Chapter 4.

The verifications and comparisons of the various data sets collected are discussed in Chapter 5 along with other discussion about the data. As the package was not finished to completion, the future developments that are required to make this package whole are indicated in Chapter 6. There were five systems that were not implemented; wireless communication capabilities, the GPS time synchronization, power independence, and total assembly. Chapter 6 describes the measures that need to be taken to complete the sensor package.

Chapter 2

Finite Element Model (FEM)

2.1 Introduction

2.1.1 Background of the Claiborne Pell Bridge

The Pell Bridge is 10,3471 in total length and has a main span on 1,601 feet making it the 83rd largest suspension bridge in the world. Traffic from Aquidneck Island would otherwise have to drive around the bay through Providence if the Newport Bridge did not exist. The original proposal for the bridge was submitted in 1950 by the designer of the New York City subway system and the Cape Cod Canal, and was approved in 1965. The concrete footings that support the two towers are supported by 838 driven steel piles. At a water depth of 162 feet the foundation created for the Newport Bridge involved the deepest pile driving in the world at this time. To accelerate cutting the tops of the piles, a dive tank was sunk that housed the divers for weeks at a time. Barges brought prefabricated sections of the bridge to Newport where they were lifted into place; the largest of the sections weighted more than 400 tons and stood 10 stories high. 90,000 cubic yards of concrete were poured into the 52 piers [18]

2.1.2 Introduction to FEM

A finite element model analyzes the physical response of a system to dynamic or static loading. The system is divided into finite elements and material structural properties are applied. The physical response of the structure to an applied loading is added to the initial configuration of the structure. Abaqus is a computer software which calculates approximate non linear finite element solutions for displacements, deformation, stresses, forces, etc. . The state of the model is updated throughout the analysis steps and the effects of the previous step are included in the solution to each iteration [19]. The stiffness matrix and friction between elements are considered in its original state and updated after each iteration. [20]

To verify the software the analysis of a simple system can be completed analytically and compared with the results of the program. For a simply supported beam the modal shapes are trivial, however, the modal response for a complex structure, like the Claiborne Pell

Bridge, anticipating modal response is near impossible with analytical solutions.

Abaqus provides multiple ways to model a particular structure. When modeling the Claiborne Pell Bridge it will be necessary to use the physical properties, such as area and modulus of elasticity, rather than the moment of inertia, to model efficiently. To ensure that Abaqus is calculating moment of inertia as anticipated, analytical solutions can be compared with the results modal frequencies of the Abaqus model. Abaqus allows for two different options of modeling, inputting the moment of inertia or imputing the profile of the element and allowing Abaqus to calculate moment of inertia.

Within a model produced in Abaqus, the removal of members allows for the structural integrity of the structure to be evaluated as an incomplete system. Future construction can be aided by this as the ability to see if a partial structure can support itself. The loss of structural components can be evaluated if lost as well. If a tower were to be damaged by a boat or a hanger were to fail, the resulting repercussion could be evaluated.

2.2 Abaqus FEM Verification

2.2.1 L Beam Analysis

As Abaqus is solving Euler-Bernoulli beam theory equations and iterating the solution over a system, if the system is simple the analytical solution can be found by hand. For the modal analysis of the 6.8 meter L beam, the beam was modeled two different ways in Abaqus. This was done to confirm that Abaqus calculates the mode shapes and associated frequencies properly. The analytical solution was calculated using Equation 2.1.

$$F_n = \frac{1}{2\pi} \left[\frac{n\pi}{L} \right]^2 \sqrt{\frac{EI}{\rho}}, n = 1, 2, 3 \dots \infty \quad (2.1)$$

The beam was modeled in Abaqus as 6.8 meters long, with the supports 0.35 meters from either end. There is a tri-axial restriction boundary condition at one end and a vertical restriction boundary condition at the other. For the initial model, an undefined profile was used and the moment of inertia and cross sectional area were input. In the second model, a preset profile was used and Abaqus calculated the moment of inertia. Thickness and outer dimensions of the beam were input. A comparison of the results of those models are presented along with the solutions to the analytical calculation in Table Table 2.1

Mode	Analytical Values	General Profile Abaqus Model Frequency	Input Profile Model Frequency	Abaqus Frequency
1	3.1 Hz	3.1 Hz	3.1 Hz	
2	12.4 Hz	12.5 Hz	12.4 Hz	
3	27.9 Hz	27.8 Hz	27.8 Hz	
4	49.6 Hz	48.8 Hz	48.6 Hz	
5	77.5 Hz	74.5 Hz	74.4 Hz	

Table 2.1: *Comparison between Abaqus models*

The frequencies of the analytical solution and the Abaqus model are very close. This is very important to the progression of this project as Abaqus must be trusted to calculate the moment of inertia within the program, translating to correct modal shapes and frequencies. Because the corresponding frequencies for the first 5 modes are more than three orders of magnitude larger than that is expected of the Claiborne Bridge (0.155-0.993Hz vs 17.6-230.1Hz), and intentions for the beam were to test accelerometer setups to be used on the bridge, analysis was not continued on the I-beam and the L-beam was introduced.

2.3 Claiborne Pell Bridge Model

2.3.1 Modeling Large Suspension Bridges

The complexity and variability of large suspension bridges makes both numerical and experimental methodology very difficult and requires many assumptions. As material and construction technologies advance, so do the length and structural complexity of these structures. Monitoring and measuring the structural integrity of these bridges is very important as fatigue is very difficult to measure and quantify. Of the failure endured by steel structures, 80-90% are related to fatigue [2]. Fatigue analysis includes evaluating the distribution of stress in structures.

Long suspension bridges are very flexible and lightly damped structures that are largely impacted by the dynamic loading of cars, wind, and environmental factors. Fatigue damage will result in large infrastructure due to long-term cyclic loading in a corrosive environment [2]. As with many bridges that experience extreme season change, the Claiborne Pell Bridge is subject to varying temperature change, snow loading, and salting in addition to the range of other challenges.

2.3.2 Modeling Process

The purpose of the analysis of the model in Abaqus is to understand the bridge behavior during static loading. As the physical properties of the bridge structural elements must be reflected in the model, the method of translating the blueprint in Abaqus properly is vital to producing accurate results. The main span of the Claiborne Pell Bridge was modeled in MKS (meter, kilogram, second) units. Each of the 8,233 elements were given the appropriate

dimension and material properties to reflect the beams and cables the Claiborne Pell Bridge. There are five structural components of a suspension bridge which will be discussed in detail:

1. Main cables
2. Towers that support the cable system
3. Hanger cables
4. Anchor bolts that support the cable system at the ends of the cable
5. Hanger cables that connect the main cable to the deck
6. Girder

Main Cables and Hanger Cables

Suspension bridges are the lightest bridges per foot made possible because by the weight bearing abilities of the cables which consist thousands of pencil-thin steel wires; that is stretched into wires and can withstand more stress. The tension force applied to the bridge girder are transferred to the main cables through the hangers. The cables are very still and flex very little but need to allow for dynamic loading and vibrations [20]. The hanger and main cables are very complicated to model as they must be modeled with the anticipation that after loaded they will accurately represent the physical shape and rigidity of the actual cables. It is now routine to measure the actual initial stresses in the hangers and main cables upon construction to input into Abaqus for Eigenvalue analysis. It is imperative that this value be accurate because initial stress in the hangers and main cable will significantly affect the structural stiffness matrix, K . The Eigenvalues were calculated as follows:

$$(2\mu[M] + \mu[C] + [K])\Phi = 0 \quad (2.2)$$

Where $[M]$ is the mass matrix, $[C]$ is the damping matrix, and $[K]$ is the stress matrix, μ is the eigenvalue, and Φ is the eigenvector [20].

Towers

The steel towers are subjected to compressive forces induced by the main cables. They need to be sturdy enough to resist buckling, oscillations, and flexing. The materials of towers is typically steel but in appropriate environments, concrete enforced steel is chosen. The current speed, price, appearance, and whether salt water or fresh water is being gaped will depict what material is chosen [20].

Anchor Bolts

Anchor piers bear the weight of the main cables and fix them in place. The anchor piers for the Claiborne Pell Bridge are 40x50x100 feet above the MWL and weigh approximately 3,950 tons each. The weight of the anchor piers hold the cables in place.

Girder

The function of the girder is to stiffen the roadway and support the road deck which carries traffic. The girder is very stiff and thus inhibits large variations in the road deck as concentrated loads travel over the bridge.

It was the unfavorable trapezoidal shape of the girder that lead to the collapse of the Tacoma Bridge in 1940. The span to width ratio and shape allowed wind excite the bridge dramatically. After the collapse of the Tacoma Bridge the girder shapes were made to be more stiff with diagonal supports and square rather than sharp edged [20].

Modeling Technique

The suspended portion of the Newport Bridge was modeled in three dimensions with an Abaqus input file. The model is made up of nodes and elements. The nodes are coordinates that define the location of the connection points of each element. The elements represent beams or beam segments. In total, 3198 nodes and 8233 elements were used to model the suspended portion of the bridge. This includes the towers from the concrete base to the top of the towers, and the main and hanger cables, roadway and truss for as far as the roadway is suspended. The cables at either end of the suspended portion and the base of the towers are modeled as fixed in all axes of translation and rotation (encoder). The towers are made up of 50 nodes and 62 elements to describe the various sections and connection points. The links and pins connecting towers to the girder (truss under the roadway) consist of 14 nodes and 22 elements. The main cables were modeled using a second order polynomial fit for the center span and a fourth order polynomial fit for the side span. The lower portion of the hanger cables and roadway are described by a second order polynomial fit in the center span and a constant 4.6 % grade outer span. The cables consist of 148 nodes for the main cables and upper connection points of the hanger cables. The lower connection points of the hanger cables are connected to nodes along the truss. The main cables consist of 152 elements

2.3.3 Limitations of Abaqus Model

Although finite element analysis has enables engineers and scientists gain an understanding of a structure's behavior and dynamic response, it is very important to know the limitations of finite element modeling. Abaqus must be used as a research tool and not considered the basis of design [19]. When verifying experimental data, a FEM should not be used for analysis as too many variables that can not be measured or controlled.

In phase one of this project, when indicating a particular profile, the preset profiles that are available do not match identically with the profiles that were used in experiments. The taper of the flange and the radius of the angle were not taken into account in the profile provided by Abaqus. As the resulting frequencies for the two different modeling techniques were not considerably different, the error acquired within the dissimilarity is assumed not to be significant and thus neglected in evaluations.

In phase two of this project, many assumptions and simplifications were made to allow for preliminary modeling. The method of modeling for this semester does not consider mated elements; the entire structure is considered as one highly elastic structure with varying physical properties rather than many different pieced welded or joined with bolts. This affects

how the bridge moves as no friction between parts and no welds are considered. Fatigue damage is local failure which occurs most often in welded regions and thus the model should include the detailed welded region connection points. The stress fluctuations are very low so the structure will deform elastically except in the welded regions. Critical locations for fatigue damage can be identified by global stress estimation [20]

Chapter 3

Instrumentation Package

3.1 Introduction

3.2 Introduction

The sensor package created this semester is a primitive prototype with bare functionality with respect to the final product. The final product sensor package is planned to be an autonomous sensor package capable of transmitting strain gauge and accelerometer data wirelessly to a base monitoring station. The package will also be synced with other sensors monitoring the same structure so the base station can collect synchronized data from multiple locations on the structure.

The package that has been developed at this stage of the project does not have some of the important functionality that the final project is expected to have. Phase 1 prototype has the ability to collect strain gauge and accelerometer data over a sampling period at a given sampling rate. The timing of the data collection was driven by an external clock source. Each sample is given a timestamp with a GPS device and logged to a file for manual analysis. At this point in time, multiple packages were not time synchronized, nor were wireless communications possible. This current package is quite modular, and has mulyiple sub-systems, detailed in the following sections.

3.3 Microprocessor

At the core of the sensor package is the microprocessor. The microprocessor served as the data collection and distribution device. The module received data from the peripheral devices and either stores the data for further analysis or distributes it in some manner. However, because of both the project requirements and the diversity of the sensors, choosing the right microprocessor meant looking closely at all of the requirements for operation. These requirements may be seen below.

3.3.1 Necessary Specifications

Power Consumption

Though power was not a focus of this semester, the microprocessor of choice was to be used through the next semester as well. This means the module of choice should be low power and made for embedded applications.

Timing Accuracy and Synchronization

The ability to time synchronize with a central clock was not a concern for the prototyping stage this semester but the same board will be used for the coming semester. In some way it must be feasible for the computer chosen to communicate with a clock source and synchronize itself. This could mean communicating with an external GPS module or with a remote NTP server.

Sampling Frequency

The microprocessor must be able to sample data from peripheral sensors at a rate fast enough to avoid aliasing data. Analysis from the Finite Element Modeling team was used to decide on this parameter

Input Output Capabilities

In order for the processor to collect and relay data from many different sensors, there are strict input output needs. To communicate with the Analog to Digital Converter (ADC), the computer needs to have an Inter-Integrated Circuit (I_2C) bus. Two Universal Asynchronous Receiver/Transmitter (UART) buses are needed to communicate with the GPS module and a wireless transmitter that has not been determined yet.

Data Logging

For testing, the ability to store data to a log file instead of exporting via wireless was desired. This allowed testing of the prototype without the use of wireless communications. The data could be collected and simply stored for later analysis.

Software Development

The platform chosen should a reasonably tested development environment and SDK. The platform chosen should have a compiler that makes use of popular languages. It should also be clear, if more than one language may be used, what the advantages and disadvantages of each approach would be. For instance, compiling an executable vs executing a python script.

Microprocessor:	BeagleBone Black 	Netburner MOD5270 
Clock Rate:	1GHz ARM Cortex-A8	145.7MHz Freescale ColdFire 5270
I/O Pins:	65	46
Power Consumption:	1.05-2.3 W @ 5V	1.65 W @ 3.3V
Data Storage:	microSD	microSD
Supported Communications:	I ² C, SPI, 3 Serial Ports	I ² C, QSPI, 3 Serial Ports
Software Development	Python,C/C++	C/C++

Table 3.1: Comparison table of two microprocessors that were looked into for the embedded sensor package

3.3.2 Platform Options

Microprocessor Comparison Table

BeagleBone Black

The BeagleBone Black is single board computer (SBC) that runs a Linux operating system (Angstrom). The board is powered by a TI AM3358 Sitara ARM Cortex-A8 Microprocessor. The core is 32 bit, and can reach up to 1 GHz clock speeds. The board comes with a plethora of pins. Included are two I_2C buses, four UART ports, and over 60 GPIO pins. There are also ground, 3.3V, and 5V pins to drive peripheral devices.

The board runs full blown Linux and root access is available. This means that development is possible with a variety of languages from C++ to Java-script More importantly, there are third party API (Application Programming Interface) libraries for the all of the board's input and output written for both Python and Java-script Both are high level languages and allow for efficient code development and quicker testing of hardware development.

Netburner MOD5270

The Netburner MOD5270 is a powerful embedded micro-controller The drawing feature of this board is the inclusion of a real time clock and its Real Time Operating System. It brings predictable multitasking and timing. Furthermore, there is an on-board SD card slot that can be used for real time data logging. The processor is a 32-bit Freescale ColdFire 5270 running at 145.7 MHz. The on-board Direct Memory Access (DMA) timers are optimal for timing the application and synchronizing data transfers. There are two UARTs and an I_2C bus to go along with various General Purpose Input/Output (GPIO) pins, including

interrupt enabled pins for external triggering if necessary.

The board has a C++/C cross compiler. The System Development Knowledge (SDK) is well documented and there are many examples for various applications. The Netburner does not run a full operation system. It runs a Real Time Operating System which handle multitasking with priority levels and cycling. This is much preferred to a full operating system for an embedded system as it makes timing more precise and the processor more efficient. However, the downside to the low level nature of the board is the development difficulty. The development is more difficult and takes more time and precision to perfect. It is also more difficult to modify than a higher level program running atop a traditional OS layer as seen in the BeagleBone Black.

3.3.3 Platform Decision

The BeagleBone Black was the single board computer chosen for the system. The system clock is fast enough to handle data at a rate of 1 kHz, the maximum sampling rate that was used for data collection. Also, there are four serial buses, so the board was able to receive data from the external GPS receiver module. Importantly, the board allowed for fast development with the Analog to Digital converter. Development would have been much slower if a different board had been chosen. The board was chosen because of its ability to satisfy all of the requirements for the microprocessor while allowing for dynamic testing throughout the prototyping stage.

3.4 Sensors

3.4.1 Accelerometer

Accelerometers were implemented in this package to determine the frequencies at which the element vibrates at. For lab testing, the desired data was the modal shapes of an L beam. The use of accelerometers for structural health monitoring is becoming common practice in smart bridges such as the new I-35W bridge in Minneapolis where periodic modal studies are performed[16].

Accelerometer Parameters

When choosing the correct accelerometer to be implemented in the sensor package, the following parameters were deciding factors:

- Number of Axes
- Dynamic Range
- Type of Mount
- Analog vs Digital Output
- Bandwidth

- Power Consumption

Number of Axes The number of axes decides how many directions that acceleration may be measured. Typically accelerometers have at least two axis. For the purposes of the sensor package, three axis were needed.

Dynamic Range The main limiting factor for determining the proper accelerometer was the dynamic range (DR). This refers to the range of accelerations that the sensor is capable of measuring. For a 3g accelerometer, the device can measure accelerations up to $3 * 9.81 m/s^2$ (or $29.43 m/s^2$). The value of the dynamic range is found on its corresponding data sheet. To determine the appropriate accelerometer, the proper DR had to be determined. This value is a dependent upon three parameters. The equation for the dynamic range, Equation 3.3 below, is dependent on the frequency being sought after and the resulting amplitude. This equation is derived from the position function, Equation 3.1;

$$u = Ae^{j\omega t} \quad (3.1)$$

$$\dot{u} = Aj\omega e^{j\omega t} \quad (3.2)$$

$$\ddot{u} = -A\omega^2 e^{j\omega t} \quad (3.3)$$

where u is the position, \ddot{u} is acceleration (or in this case the DR), A is the displacement, ω is the measured frequency in radians, and f is the frequency in Hertz. This equation allows one to calculate the allowed maximum displacement before reliable data cannot be measured. Since the frequency value of the acceleration function is squared, a change in frequency will cause a dramatic change in the maximum allowed amplitude. Using a maximum frequency of 77.5 Hz (determined analytically by the FEM team for the simply supported beam) and a 1.5 Hz frequency (a rough representative of the Newport Bridge), the maximum displacement of a structure before unreliable data acquisition occurs was calculated for every accelerometer that was considered. These values are shown in Table 3.2.

Type of Mount Accelerometers can be mounted to a circuit board in one of two manors: through-hole mounting or surface mounting. An accelerometer with dual inline package (DIP) header pins can be placed directly into a breadboard for prototyping; whereas a surface mount accelerometer needs to be specially soldered to a PCB.

Analog vs Digital Output The difference between an analog and digital accelerometer is how the output data is processed. Analog accelerometers output a frequency that is proportional to acceleration whereas digital accelerometers output a square wave of a certain frequency. The amount of time that the wave is high is proportional to the amount of acceleration [7].

Bandwidth The bandwidth is defined as the useful frequency range in which the response falls to -3dB of the nominal value (0 Hz) [17]. Therefore, while choosing an accelerometer, the desired frequencies must fall within the bandwidth of the sensor.

Power Consumption To conserve power, finding an accelerometer with low current draw was essential. Fortunately most accelerometers require only a small amount of current draw.

Accelerometer Selection

The comparison of the considered accelerometers is tabled below. Initially, the AXL330 was chosen as the best option compared to the BMA220 and the ADXL362 because it is an analog accelerometer. This is because it was determined that an analog accelerometer would allow for the easiest time synchronization of data with the other sensors. However, during laboratory testing data was being clipped. This data was deemed unreliable because as data is clipped the response becomes a multiple derelict function instead of a single one. This causes data fitting to appear like a square wave instead of the intended sinusoidal wave. Therefore the MMA7361L accelerometer was used in place of the ADXL330.

Parameter	Accelerometer Model				Units
	BMA220	ADXL362	ADXL330	MMA7361L	
Analog/ Digital	Digital	Digital	Analog	Analog	
Dynamic Range	$\pm 2/4/8/16g$	$\pm 2/4/8g$	$\pm 3g$	$\pm 1.5/6g$	m/s^2
Maximum Displacement @ 77.5 Hz	0.083/0.165/0.331/0.661	0.083/0.165/0.331	0.124	0.062/0.248	mm
Maximum Displacement @ 1.5 Hz	220.9/441.7/883.5/1766.9	220.9/441.7/883.5	331.3	165.7/662.6	mm
Bandwidth: X & Y-axis	32/64/125/250/500/1000	50/200	0.5-1600	400	Hz
Bandwidth: Z-Axis	32/64/125/250/500/1000	50/200	0.5-550	300	Hz
Current Draw	250 @ 3V	3 @ 2V	320 @ 3V	400 @ 3.3V	μA
Power Consumption	750	6	960	1320	μW
Number of Axes	3	3	3	3	

Table 3.2: Comparison table of four accelerometers that were possible candidates for the sensor package.

3.4.2 Strain Gauge

The deformation and displacement that an object feels under an external force is defined as strain [6]. In the applications of engineering and construction the strain of an object, such as a support or beam, is a necessary component to monitoring the structure. To measure the strain of a structure, a strain gauge may be applied. The strain gauge can be a very effective measurement technique for SHM because it has the ability to measure the compression and expansion within the members of the structure. The strain values measured on the structure can be used to state the stress within the material to monitor and predict the safety of the structure. The change in capacitance, inductance or resistance is proportional to the strain experienced by the sensor. The strain sensitivity or gauge factor is a dimensionless figure that represents the tolerance of the gauges . It allows for the gauge to have minimal imprecision for changes in temperature. Equation 3.4 shows the calculation of the gauge factor (GF) for a strain gauge

$$GF = \frac{\Delta R/R}{\epsilon} \quad (3.4)$$

Where ϵ is the lateral or longitudinal strain; defined by 3.5.

$$\epsilon = \frac{\Delta L}{L} \quad (3.5)$$

Ideally strain would only change due to a change to the surface on which the sensor is attached to. However, temperatures, material properties, the bonding adhesive and the stability of the metal all affect the detected resistance. So when selecting a strain gage one must be thorough in understanding the conditions the gage may be under during use. Because material properties are not the same in each direction, knowing axial strain is not sufficient. Poisson strain and shearing strain of the material are required to calculate the principal strain. Poisson strain is both the thinning and widening of the beam, as well as the elongation that the beam may feel under strain. Shearing strain is the angular distortion of the beam, or the angle of rotation or twist due to shear stress. Generally, to calculate the principal strains the largest normal strain is of most interest. This can be found by taking the derivative of ϵ_X or ϵ_Y with respect to θ and equating it to zero. This gives the principal rotation angle, θ_p , this will help produce the principal strains (max and min); as seen in Equations 3.6 - 3.8

$$\epsilon_{p,q} = \frac{1}{2} \left[\epsilon_1 + \epsilon_3 \pm \sqrt{(\epsilon_1 - \epsilon_3)^2 + (2\epsilon_2 - \epsilon_1 - \epsilon_3)^2} \right] \quad (3.6)$$

$$\sigma_{p,q} = \frac{E}{2} \left[\frac{\epsilon_1 + \epsilon_3}{1 - \nu} \pm \frac{1}{1 + \nu} \sqrt{(\epsilon_1 - \epsilon_3)^2 + (2\epsilon_2 - \epsilon_1 - \epsilon_3)^2} \right] \quad (3.7)$$

$$\Theta_{p,q} = \frac{1}{2} \tan^{-1} \left(\frac{2\epsilon_2 - \epsilon_1 - \epsilon_3}{\epsilon_1 - \epsilon_3} \right) \quad (3.8)$$

The towers of the Newport Bridge stand 400 feet tall, the suspended structure consists of over 23,000 tons of steel, the total length of the wires is close to 8,000 miles, and the amount of concrete used in the substructure is 136,000 cubic yards [21]. There are many aspects of the

bridge that can be damaged; the best process to minimize the damages that may occur is to inspect the structure as often as possible and make repairs in a timely manner. Implementing strain gauges to monitor the structural health of the bridge is the most economical procedure to continually collect data to assess if structural changes have occurred. For the design group to collect accurate strain measurements that can be analyzed to assess the bridge's health, bonded foil strain gauges were used. Imaged below is a figure of a 3-element strain gauge.

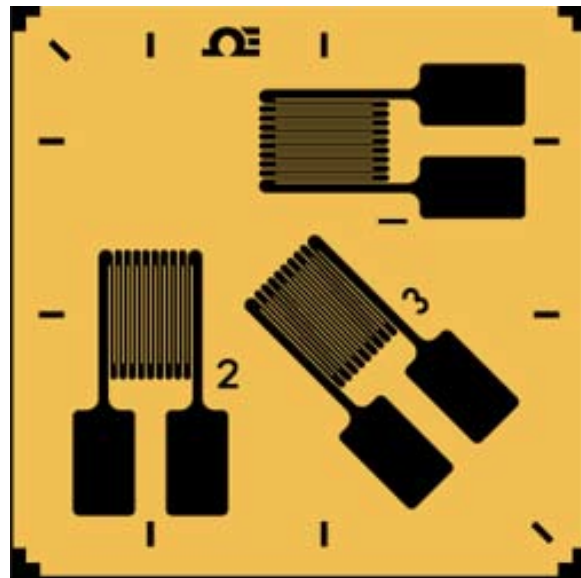


Figure 3.1: *3-Element Rosette, metal-foil type strain gauge*
Manufacturer: Omega

The typical metal foil-type strain gauge consists of a grid of wire filament that acts as a variable resistor. The gauge is bonded onto the surface of the structure by using an epoxy resin specific to the structure material. When the structure is under strain the change in surface length results in a change in the resistance, this change in electrical resistance in the foil varies linearly with strain. To obtain strain with a metal foil-type strain gauge a Wheatstone bridge must be utilized to measure the small changes in resistance due to strain. A Wheatstone bridge is a divided bridge circuit used for measuring static or dynamic electrical resistance. The Wheatstone Bridge utilizes the difference in resistance from each half of the bridge to either produce a voltage differential when measured from one half of the bridge to the next.

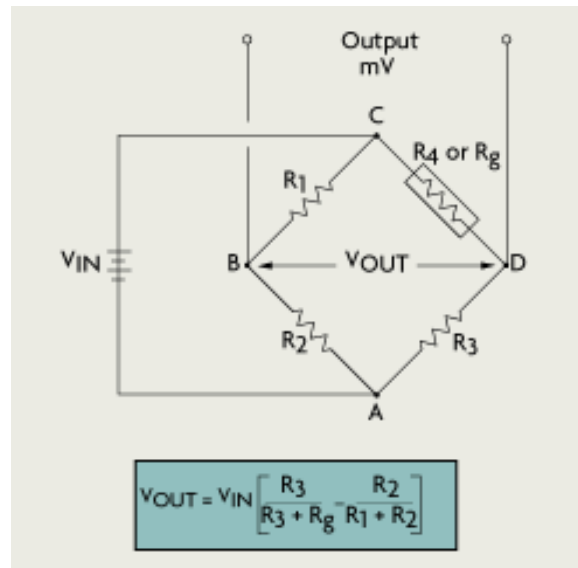


Figure 3.2: Wheatstone Bridge Circuit Schematic[6]

For the sensor to accurately measure the strain of the proposed test beam, the group needed a 3-element rosette with a nominal resistance of 120Ω , max permitted bridge energizing voltage of $12V_{rms}$ that was matched to aluminum, and a maximum strain of 30,000 micro strain ($\mu\epsilon$). The strain gauge originally selected was the SGD-6/120-RYT83.

3.4.3 Strain Gauge Selection

The primary factors that influenced the strain gauge selection were:

- Operating Temperature
- State of Strain
- Stability of the Metal Foil
- Gauge Factor
- Power Consumption

Operating Temperature The service temperature of the strain gauges needed for our project must be versatile. The service temperature for the gauges purchased range from -100°F to 392°F .

State of Strain The nature of the strain for this project was mostly axial strain. There was also bending strain from the force of the load applied during testing as well as shear strain determined by measuring the strain at a 45° angle. The 3-element rosette allowed for the sensor to measure all three types of strain at once.

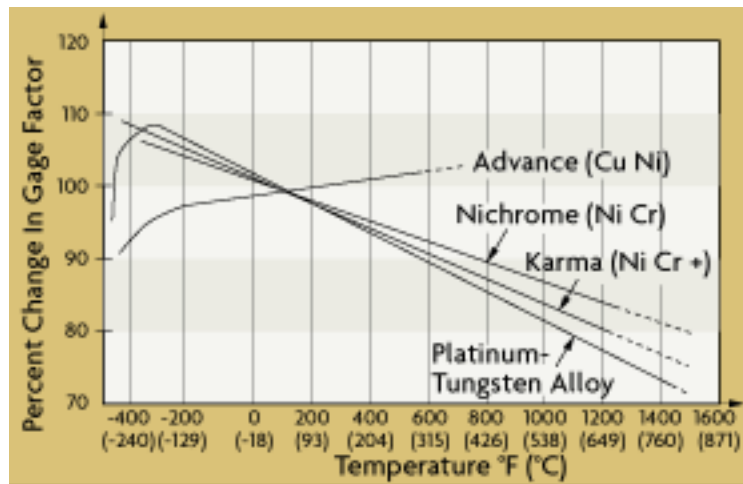


Figure 3.3: Graph showing the relationship between gauge factor and temperature change[6]

Stability of the Metal Foil The stability of the metal foil measuring grid is important because the electrical resistance must be measured accurately on a consistent basis. The strain gauge applied in this project uses a 5-micron thick constantan foil. Constantan is a copper, nickel alloy that is most often the type of metal foil used within a strain gauge because of its consistent gauge factor which is highly dependent on temperature with other metal foils such as Karma which is a nickel, chromium alloy.

Gauge Factor The gauge factor or strain sensitivity of a sensor is the proportionality factor between the relative change in resistance . The gauge factor chosen varies less with change in temperature than other types of gauges, this can be seen by viewing the Copper Nickel curve in Figure 3.3. The sensor used for the package had a gauge factor of 2.0.

Power Consumption The power consumption of the gauge is mostly a result of the needed connection to the Wheatstone Bridge. The quarter bridge circuit consumes 27.5mA at 3.3V, or 90.8mW.

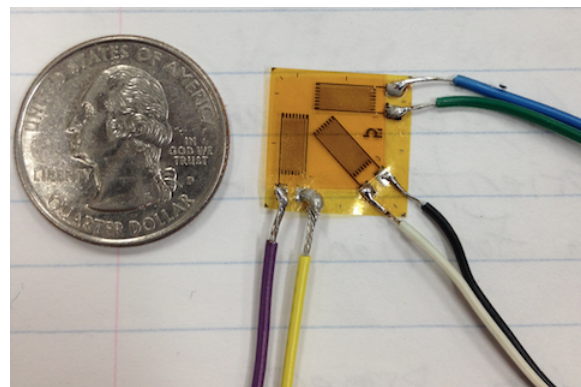


Figure 3.4: Omega 3-Element Rosette with leads attached

Figure 3.4 pictured above is the one of the original 3-element rosette strain gauges with wires soldered to the solder pads. Due to the small solder pads, it proved to be difficult to achieve secure solder joints. It is likely that the gauges were damaged upon soldering the wires to them because of the poor data that was collected from them. To arrest these issues the group purchased strain gauges with the leads directly connected to the solder pads. Purchased from omega engineering, the model number was SGD-6/120RYT23. These gauges included ribbon leads, however when attaching clips to the leads during experimentation the leads came undone. Despite the troublesome attempts to get the strain gauges working, once they were connected correctly there was still no accurate data received. A strain gauge with a different gague factor or a higher resistance would be more appropiate.

3.4.4 GPS Receiver

The need for an accurately synchronized timing system was present throughout the planning of the sensor package in order to synchronize data from multiple sensor packages. The internal clock on the microprocessor board was determined to be unreliable due to inherent errors from low tolerances in CPU clock crystals. The use of a GPS receiver as an external timing source was explored [15].

GPS Parameters

The following parameters were considered when choosing the GPS receiver for time-synchronization:

- Power Consumption
- Pulse Per Second (PPS) Output Signal
- Communicate via Serial Interface

Power Consumption As for all other components in the sensor package, the GPS needed to have a low power draw. The GPS receiver was anticipated as being the sensor with the highest power consumption.

Pulse Per Second (PPS) Output Signal It is proposed for future use that the PPS signal be used for time synchronizing the data between multiple sensor packages.

Communication Due to the communication protocols that the microprocessor supports, found in Section 3.3, the GPS must support UART, SPI or I²C communications as inputs.

Sensor Selection

The Trimble Copernicus II (Figure 3.5) is a 12-channel, PCB mounted GPS. The GPS features two serial ports and a 3.0v PPS output signal, shown in Figure 3.6. The power consumption of the package is approximately 132mW at 3V. This receiver was chosen as a prototyping solution because it was available in a dual in-line package (DIP), making it easily interfaced on a breadboard.



Figure 3.5: *Copernicus II GPS receiver*

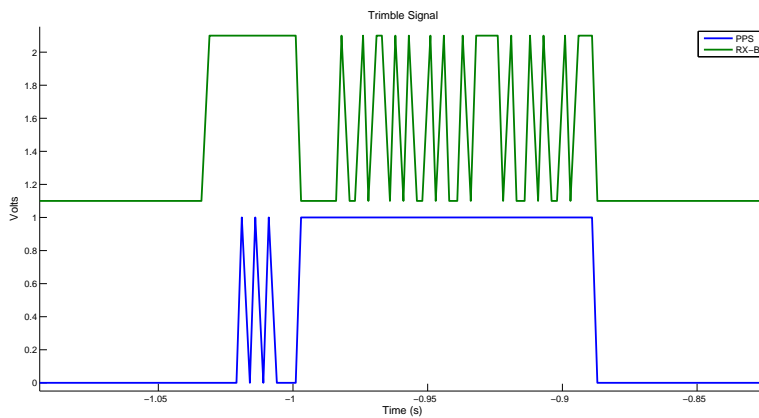


Figure 3.6: *GPS sentence data and PPS signal recorded with oscilloscope for preliminary analysis.*

3.4.5 Analog to Digital Converter

Necessary Specifications

The BeagleBone Black microcontroller features an on board 12-bit analog-to-digital converter (ADC). From literature, the lowest acceptable effective resolution that an ADC being used for SHM may have is 16 bits[3] [12]. It was determined that the need for an external ADC was present. The parameters of the external ADC needed were as follows:

- High Resolution
- Appropriate Sampling Frequency
- Low Power Consumption
- Support for Multiple Input Channels
- Communicate via Serial Interface

Resolution Resolution is defined as the number of bits that an analog signal is mapped to after being converted[13]. Using the chart in Figure 3.7, it was evident that in order to achieve high resolution data that a Delta-Sigma ($\Delta\Sigma$) ADC needed to be used.

As previously stated, the minimum resolution required for this sensor package was 16-bits. The voltage resolution can be found using Equation 3.9:

$$V_{Res} = \frac{V_{Range}}{2^n} \quad (3.9)$$

Assuming $V_{Range} = 3.3V$, $n = 16$ bits then V_{Res} is approximately $50.35\mu V/\text{division}$.

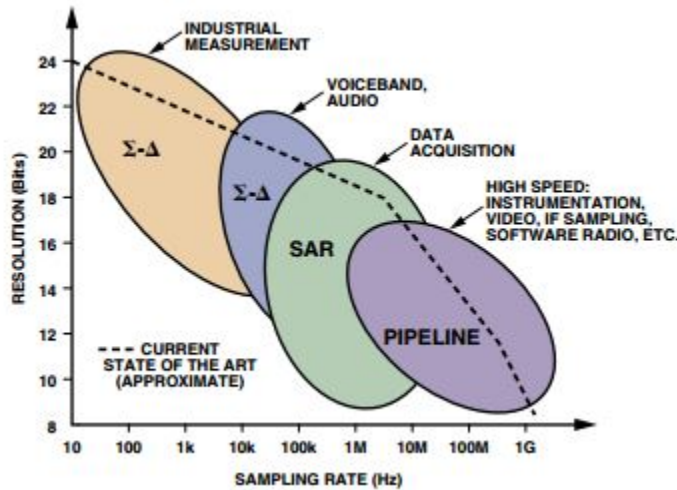


Figure 3.7: Chart displaying the classifications of different ADC architectures [14]

Sampling Rate The Nyquist-Shannon Sampling Criterion states that data must be sampled at a minimum of twice the expected frequencies being measured [13]. The accelerometer that was chosen for the preliminary lab experiments has a bandwidth of 500Hz , therefore the ADC must be able to sample a minimum of 1kHz . However, since frequencies expected from the lab testing are in the range of $0 - 60\text{Hz}$, the sampling frequency of the ADC does not necessarily need to be so high.

Power Consumption Since the nature of this sensor package was to be a wireless sensor, it was assumed that all power used by the sensor package would be generated using alternative energy. With this in mind, components used on board the sensor package have as little current draw as possible.

Input Channels One important, but almost overlooked, characteristic of the ADC was the ability to support multiple input channels simultaneously. The ADC needed to be able to read three channels from an accelerometer and at least two channels from a strain gauge. For prototyping purposes, it is typically difficult to find ADC's with more than 4 inputs; most come in as surface mount components and require a printed circuit board. It became evident as the project progressed that each input device would need a dedicated ADC due

to the multiplexer switching time of multi-channel ADC units. It was decided to address this problem by interfacing four ADC units simultaneously on a serial communication bus. Subsection 3.4.5 discusses this in further detail. It should also be noted that the inputs of the ADC were configured for differential measurements. This gives the ability to compare the sensor data to a noise reference, and thus make reducing data filtering during processing.

Communication As shown in Table 3.1, the BeagleBone Black supports multiple communication protocols, include but not limited to, SPI and I²C. The communication from the ADC to the main micro-controller was decided to be either 4-wire SPI or I²C. The ADC will be the slave to the micro-controller. A con using SPI as the communication method is that for each slave device in the communication loop, there must be a dedicated Slave Select (SS) line. This puts a limitation on how many ADC's can be used in each sensor package. However, I²C utilizes a central bus and 7 bit unique addresses for slave selection.

Analog-to-Digital Converter Selection

When searching for ADC's that fit the parameters set in Section 3.4.5, three devices were investigated; the TI ADS1211, TI ADS1115 and the TI ADS1113. The devices are summarized in Table 3.3 and explained in detail below.

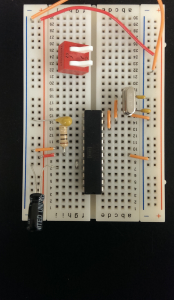
Parameter	Analog-Digital Converter		
	ADS1211	ADS1115	ADS1113
Package			
Resolution:	24 bits	16 bits	16 bits
Supported Communications:	SPI	I ² C	I ² C
Power Consumption:	5mW @ 5V	0.66 mW @ 3.3V	0.66 mW @ 3.3V
Number of Inputs:	4	4	1

Table 3.3: Comparison table of the ADS1211, ADS1115 and ADS1113 ADC devices

TI ADS1211 The Texas Instruments ADS1211 24-Bit ΔΣ analog to digital converter features 20 effective bits of resolution at 1kHz under ideal conditions; however that would be contingent upon the ability to design an ideal printed circuit board (PCB) for the converter.

Between 16 and 18 bits of resolution are realistic for the initial prototype of the sensor package. By utilizing an internal 4-to-1 multiplexer, four input channels are available to use. Recall that Section 3.4.5 requires at least five input channels, the ADS1211 falls short here. As a solution two ADC's would be used, making it possible to read two strain gauges per sensor package as opposed to one. The ADS1211 datasheet provides information on synchronizing multiple ADC's together. The converter draws approximately $10mA$ under typical working conditions. The converter utilizes the SPI protocol that is supported by the BeagleBone Black.

The ADS1211 was purchased and interfaced; however due to the complex circuitry that was required by the device, a month passed before the chip was tested. The converter functioned correctly for approximately ten minutes and then stopped transmitting data.

TI ADS1115 The Texas Instruments ADS1115 16-Bit analog to digital converter is of the same architecture as the ADS1211 ($\Delta\Sigma$). The chip also features a multiplexer that allows up to 4 single ended or 2 differential inputs. The sampling frequency of the ADC is programmable from 8Hz to 860Hz, and includes an internal oscillator. The average current draw for the ADS1115 is approximately $150\mu A$. There are two notable differences between the ADS1115 and the ADS1211 ADCs. First, the ADS1115 communicates via the I²C communication protocol. The ADS1115 has four unique I²C addresses; making it possible to have 16 single-ended inputs on one communication bus. Also, the chip was available pre-mounted on a PCB with all the necessary supporting hardware; thus eliminating the possibility of incorrectly wiring up the circuit.

TI ADS1113 The TI ADS1113 is within the same family as the ADS1115, only differing in the number of input channels and not having internal programmable gain amplifiers and comparator. Like the ADS1115, four ADS1113 units can be on the same I²C bus, can also run in continuous sampling mode, and also shares the same library of functions as the ADS1115. Since the ADS1113 does not multiplex its inputs, there is no loss of data between switching. The disadvantage to the ADS1113 is that it is only available as a surface mount chip (MSOP-10 package); thus requiring more circuitry on the printed circuit board.

ADC Impedance Matching Preliminary lab tests were performed using a micro-controller with 12-bit ADC to collect data for analysis. The time series that was returned did not accurately represent the data present, as verified with an oscilloscope. It was determined that this was due to a difference in impedances between the accelerometer and the ADC. The solution was to construct an op-amp circuit to match the impedances of the accelerometer and the micro-controller inputs. It was initially believed that the internal programmable gain amplifiers (PGA) of the ADS1115 would avoid such issues in impedance matching. However, after further research it was discovered that this assumption was incorrect.

ADC Final Selection Based on the comparison of the ADS1211, ADS1115 and ADS1113 ADC's, the ADS1115 was chosen for the preliminary package to test code before the printed circuit board was designed. For the final package, four ADS1113 ADC units were integrated into the PCB design as discussed in Section 3.5.2.

3.5 Electrical Design

3.5.1 Introduction

The unique requirements for the sensor developed for deployment on the Claiborn Pell Newport Bridge set the sensor apart from off-the-shelf sensors readily available for purchase. The sensor package needed to record high precision, high resolution accelerometer and strain gauge data continuously for an extended period of time. The longevity of the package was dependent upon the battery capacity and data storage capacity. This could have been solved by utilizing a large bank of batteries and multiple hard disk drives; however it was determined that this was not a feasible option. Instead the sensor package would scavenge energy to recharge batteries and transmit data to a base station wirelessly. The addition of these two requirements greatly increased the complexity of the sensor package design.

3.5.2 Circuitry

Voltage Regulation

The voltage input for most systems on the sensor board are a range of voltages between 3.3V-5V. This posed a basic issue due to the output voltage of the 12V battery. The solution was to use two LM317 linear voltage regulators. It was initially proposed to use the two regulators in series, such that the voltage dropped from 12V to 5V and then to 3.3V. However, due to the current rating on the devices, it was decided to use the regulators in parallel and drop the voltage from 12V to 5V and 12V to 3.3V. The complete circuit may be found in Appendix A.1. The LM317 technical specifications are displayed in Table 3.4

Parameter	Value
Input Voltage Differential ($V_{in} - V_{out}$)	$3V \leq V_{in} - V_{out} \leq 40V$
Output Voltage (V_{out})	$1.2V \leq V_{out} \leq 37V$
Output Current (I_{out})	1.5A
Max Power Dissipation (P_D)	20W
Package Type	TO-220

Table 3.4: *LM317 Adjustable Linear Regulator Specifications*

The output voltage can be set using Equation 3.10 where $R_1 = 240\Omega$ and $I_{adj} \leq 100\mu A$. It should be noted the V is not the input voltage, but a unit placeholder. Since I_{adj} is very low, the error associated with it is almost negligible.

$$V_{out} = 1.25V(1 + \frac{R_2}{R_1}) + I_{adj}R_2 \quad (3.10)$$

The regulation circuit was tested using a 7.7Ah 12V battery in order to confirm the output voltages. The voltages recorded were steady at approximately 3.5V and 5.3V. The error is believed to be due to the inherent tolerance in the passive components used in the circuit.

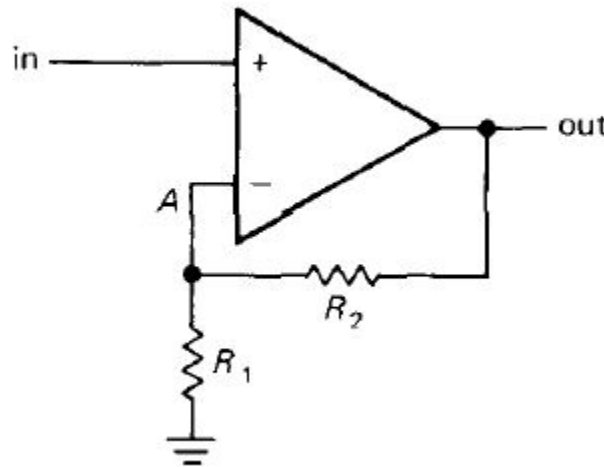


Figure 3.8: Standard configuration of op-amp as a buffer

Also in field use, the package will be subject to a wide range of temperatures that will cause the error in voltage to vary.

ADC Impedance Matching

As mentioned in Section 3.4.5, impedance matching issues were encountered when sampling accelerometer data with the micro-controller. To avoid such issues in the final design, an impedance matching op-amp was used. The MCP606 op-amp was used due to its rail-to-rail output, low input offset voltage, unity gain stability and low power characteristics. In order to act as a buffer for the input of the ADC, the op-amp was configured as in Figure 3.8; where R_1 and R_2 are governed by the Equation 3.11. Since the op-amp will be used with unity gain (gain = 1) then both resistors are 0Ω and just wired connections [10].

$$\text{gain} = 1 + \frac{R_2}{R_1} \quad (3.11)$$

Decoupling Capacitors

In order to reduce noise on the power supply line to each component, decoupling capacitors were added to each device between the voltage input and ground. Decoupling capacitors act as low-pass filters, thus removing high frequency voltage differentials. To ensure no inductance due to the transmission length between the decoupling capacitors and device inputs, the transmission length was minimized [10].

3.5.3 Printed Circuit Board

In order to combine the system in an efficient manor, it was decided that a printed circuit board (PCB) must be designed to carry the components. This would make future

sensor packages easy to manufacture for additional sensor nodes on the bridge and ensures consistency between packages. It should be noted that all schematics and circuit board files were created using National Instruments Multisim 13.0 and Ultiboard 13.0 respectfully. All schematics and board files may be found at <https://github.com/mpiannucci/SeniorDesign/tree/master/hardware>.

Requirements for PCB

Initially the requirements for the PCB were to create a carrier board that would allow for the addition and removal of package components via header sockets. This would allow for the purchase of many off-the-shelf components that would be able to be installed with minimal effort. For various reasons, the scope of the PCB was change from being a carrier board to completely integrating all of the components. This posed difficulties as many of the components utilized in the package were bought as standalone solutions with dedicated PCBs for each component. As a solution for this, all component that shipped with PCBs had all of their circuitry mimicked on the main PCB. This holds true for all components except for three; BeagleBone Black, Trimble Copernicus II GPS receiver and the XBee Pro S3B wireless receiver. It was decided that it was more appropriate to create sockets for each of these components to plug into for specific reasons. Although the board files for the BeagleBone Black are readily available to download, it was deemed unnecessary to recreate the board. For the Trimble Copernicus II GPS receiver, it was decided that because of the sensitivity in the design of the antenna circuit that it would be best to use the off-the-shelf board. The board purchased has the antenna circuit integrated with impedance matched SMA connector for the antenna. Due to unforeseen issues with interfacing the XBee Pro S3B wireless receivers, the receiver was not incorporated in the initial version of the system design. Section 6.1.2 discusses the future work to be done with the XBee Pro S3B receivers.

Progress on Printed Circuit Board

All component footprints for components in the sensor package were created in Multisim 13.0 and Ultiboard 13.0. The library of components may be found at <https://github.com/mpiannucci/SeniorDesign.git> under `./hardware/UsrComp_S_SHMComps.usr`. A basic board was laid out, however trace routing was not completed due to unresolved net issues. Although the board design was not finished, a comprehensive schematic was created and will prove useful for future development of the board. The schematics may be found in Appendix A.

3.6 Software Design

The software design controls the timing and data collection for the package. The software structure is simple, yet crucial. In order to keep the data collected by the package relevant, the software logic and timing needed to be in order.

The first state in the software design is the initialization state. Here, the analog to digital converter was initialized through I2C communication. The handle of the analog to digital

communication object was saved for later use in the next state. Once the initialization state was finished, the application proceeded to the sampling state.

In this application, 200 Hz was decided to be the target sampling rate. The program waited for an interrupt then the system time has reached a user-defined time. This is important because every sensor package waited for the same time and they sampled at the same instant (accurate to a millisecond). When the signal was received, the application proceeded to collect data from the peripheral sensors. For each sample during the sampling duration, data was collected from the ADC via I2C. The data structure was appended over the sampling entire sampling period and passed as a return from the state. Once the sampling duration was over, the data logging state was begun.

The data logging state received the data structure created in the previous sampling state. This data was then sorted and written to a standard comma delimited text file. The file stream was closed once all of the data had been written and the program finishes. A simple block diagram of this flow can be seen in Figure 3.9.

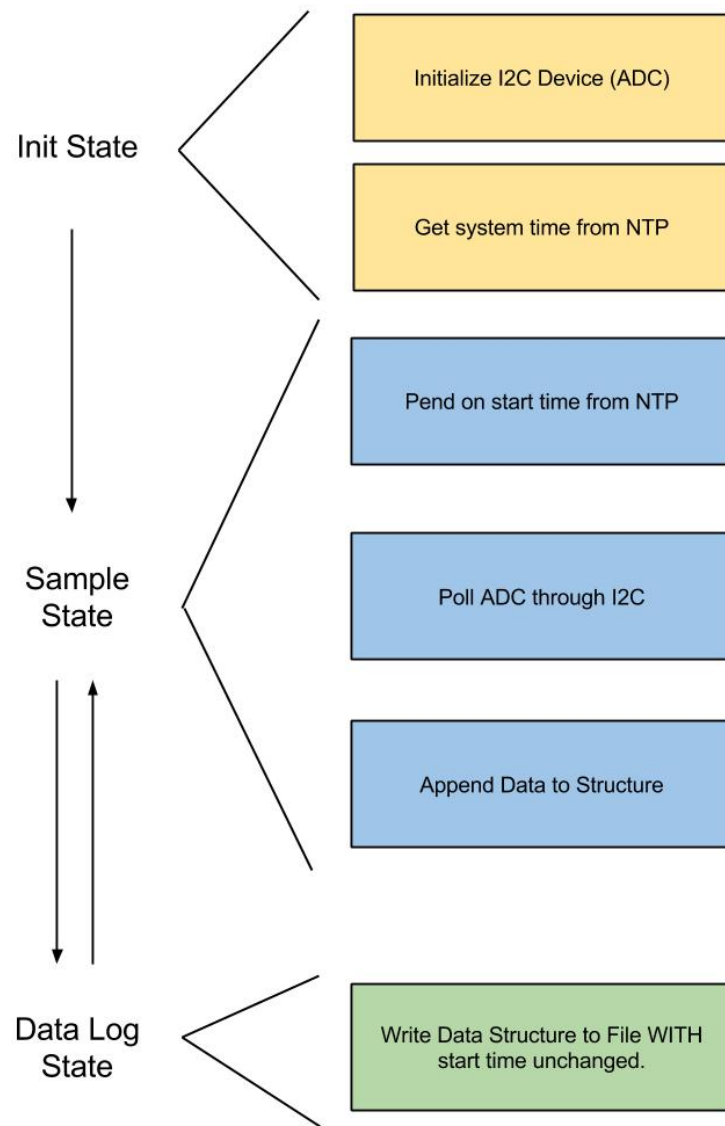


Figure 3.9: *Software flow of the sensor package*

3.7 Package Power

3.7.1 Power Budget

After analyzing the power consumption of the individual components of the sensor package, the following power budget was formed (Table 3.5). Note that there was +10% allocation added to the total power calculated. This was to account for any errors in calculation or any miscellaneous items that were looked over.

After adjusting the power budget to a more conservative value, the package is projected to be a 5 watt system. By specifying a constant power consumption, an ideal battery

Component	Power Consumption (mW)
Beagle Bone Black	2300
Analog to Digital Converter	1
GPS	132
Wireless Transmitter(Anticipated)	800
Strain Gauge	95
Accelerometer	2
Total Power	3660

Table 3.5: *Time without power production*

capacity was determined. The power values calculated for each component were under the assumption that the system would run continuously. In the future implementation of a wireless transmitter, a constant current draw of 215 mA was assumed. This value corresponds to a maximum power consumption and does not account for a possible boost in signal. For more accurate power profile, future testing should be completed using the package.

3.7.2 Package Power

Solar Potential

The package is designed for long term structural health monitoring, making energy storage imperative. Energy can be scavenged in a number of ways; the popular methods depend on the more abundant natural resources: solar and wind energy. The energy scavenging devices essential to this project are a solar panel, wind turbine, and rechargeable battery system.

The National Oceanic and Atmospheric Administration (NOAA) offers datasets for various climate properties such as humidity, temperature, cloud coverage, etc. The statistical analysis of historical data is crucial for the design of an energy storage system. NOAA offers data for the downward short wave radiation flux for the past 65 years. These files can be imported into MATLAB and refined for the values relevant to a desired location. The data is recorded for all locations around the world based on the respective longitude and latitude, Newport, Rhode Island is located at latitude (41.5), longitude (-71.3).

One year of data will show the trend of available sunlight throughout the change of seasons. It is necessary to take into account periods of time with limited sunlight such as an overcast lasting multiple days. In order to account for events of negligible sunlight over the years, solar data from 1994 through 2013 was uploaded; this data was plotted in MATLAB and is shown in figure 3.10. By averaging each daily average value over the last 20 years, a plot of expected solar radiation flux was generated for a given year. Downward short wave radiation flux is a measure of power in units of watts per square meter, this data is illustrated in figure 3.11.

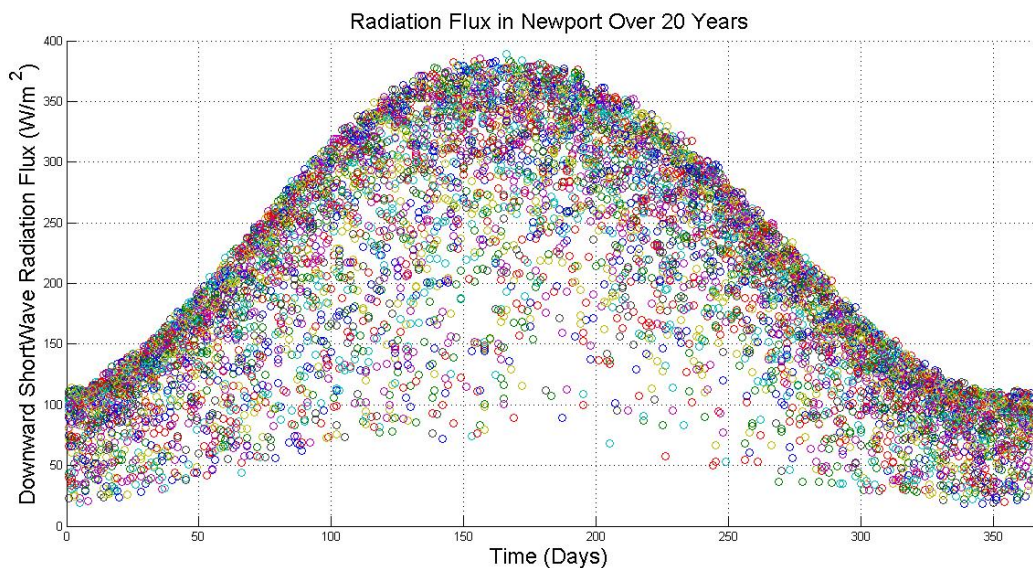


Figure 3.10: *Newport Radiation - 20 years*

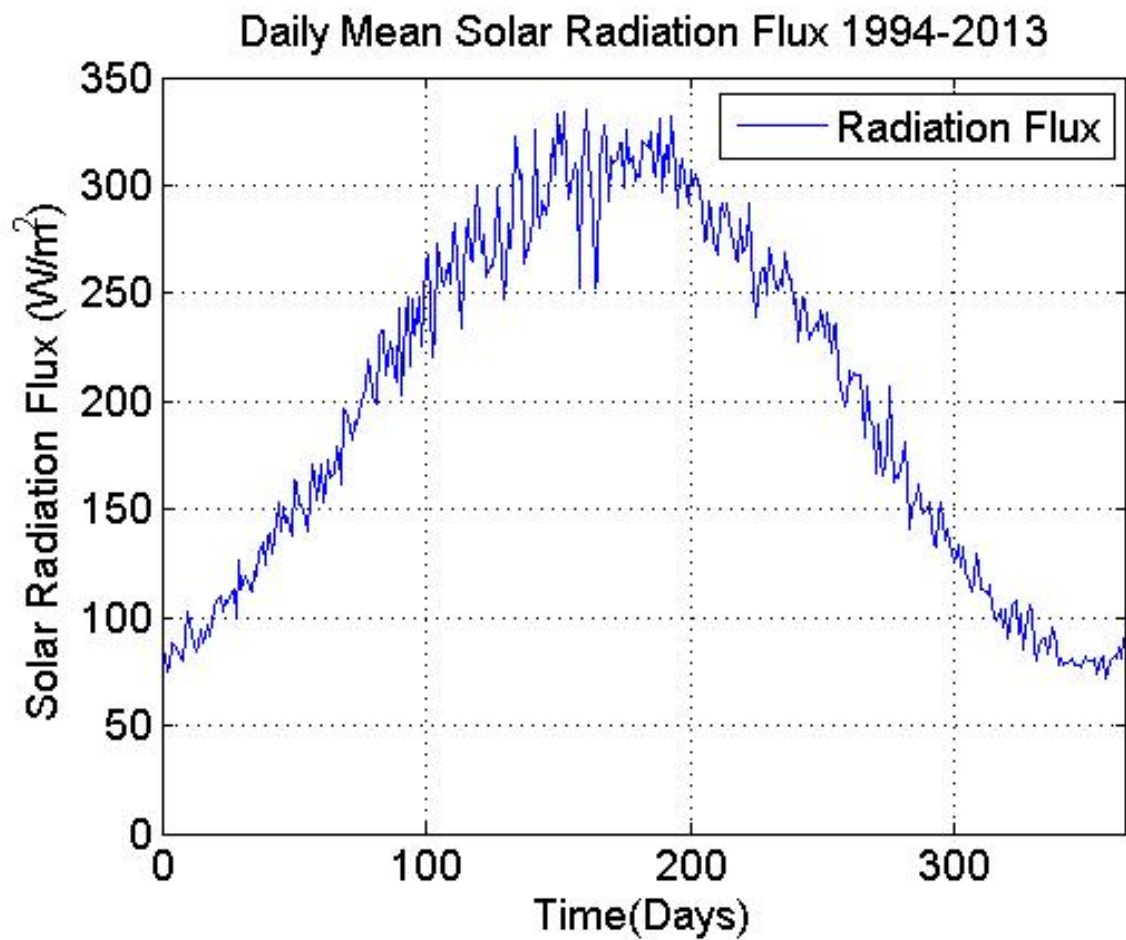


Figure 3.11: *Newport Radiation*

This project used two photo-voltaic solar panels purchased from SunForce with a maximum power rating of five watts. Solar panels power rating are directly proportional to their surface area, hence why a five watt solar panel is much smaller than an eighty watt. In order to convert radiation flux, measured in watts per square meter, to the power outputted by a solar panel, the efficiency factor of the panel must be calculated.

Solar cell efficiencies are measured conventionally under standard test conditions that correspond to a clear day with incident solar radiation. These standard conditions specify a test environment with temperature of 25°C and direct radiation flux of 1000 W m^{-2} . The ratio of the specific power rating to the radiation flux in standard conditions yields the efficiency factor, which has units of square meters. Multiplying a value of actual radiation flux that the solar panel may experience by the efficiency factor will determine the expected power output of the panel in units of watts.

$$\text{EfficiencyFactor} = \left(\frac{\text{PowerRating}}{\left(\frac{1000\text{W}}{\text{m}^2} \right)} \right) \quad (3.12)$$

This calculation can be done for the average solar radiation flux over the past 20 years which is approximately 199.7 W m^{-2} . Therefore, the average expected output power from a 5 watt solar panel is 1 watt. By implementing both solar panels in parallel, the output power doubles hence the expected output power is 2 watts. Figure 3.12 shown below illustrates the output power throughout a period of 365 days as well as plotting each daily average power minus one standard deviation. Conceptually, this statistical analysis will yield a more realistic and conservative range of values for the expected output power.

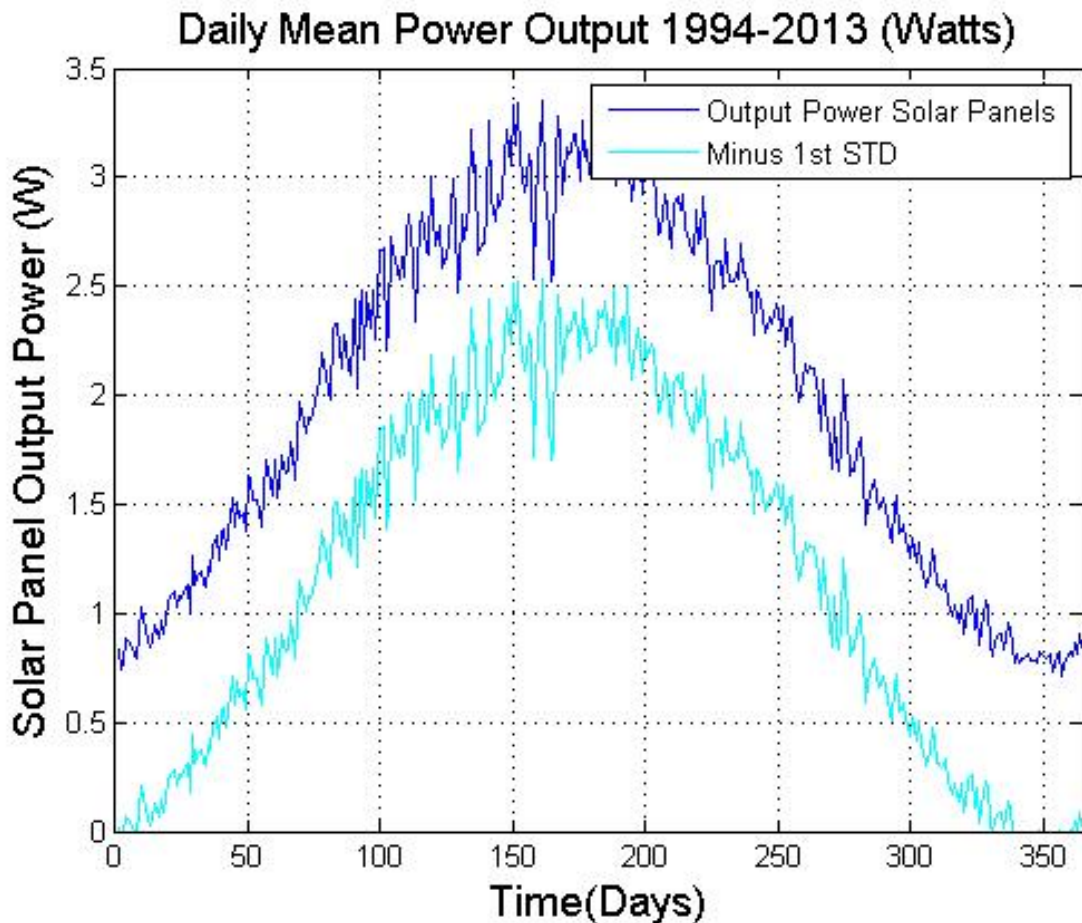


Figure 3.12: *SolarPanel*

Orientation of a solar panel depends on two things, the inclination from the horizontal, and the direction at which the solar panel faces. Solar panels mounted in the Northern hemisphere should be directed true South, and in the Southern hemisphere directed North. For optimal performance, the tilt of the solar panel should be adjusted seasonally to obtain the most energy over a whole year. For this project, it was assumed that the solar panels stay at a fixed tilt. To determine the optimal tilt above the horizontal, most articles suggest an inclination equal to the latitude, for Newport that would be 41 degrees. As previously stated, the tilt should be adjusted twice a year during the change of seasons. For the winter months, the angle should equal the latitude plus fifteen degrees, while in the summer time being angled at the latitude minus fifteen degrees. Since this is a hybrid energy scavenging system, the wind turbine will be working in tandem with the solar panels and it is expected that a majority of the energy will be gathered by the wind turbine. For that fact, the solar panels should be oriented for optimal performance during the summer season, when the wind turbine experiences the lowest wind speeds.

3.7.3 Wind Potential

The site of the Newport Bridge is a viable location for wind energy scavenging because the bridge is high off the ground and there are no sounding objects to block the wind. To harvest energy from the wind, the wind is used to turn a generator which converts the mechanical energy to electricity which is then stored in batteries. Due to expense limitations, only a single battery can be used, in conjunction with harvesting recharging techniques, to keep the sensor package running continuously for years.

NOAA has a data station in Newport, RI approximately 500 meters north of the bridge. The station has yearly data from this point and the data points are collected every 6 minutes, which corresponds to about 87,000 data points a year. The anemometer is approximately 6.4 meters off the ground.

For the wind speed to be accurate at the height of where the turbine would be placed on the bridge, the wind data has to be reconfigured. This is done with the wind profile power law:

$$U_2 = U_1 \left(\frac{Z_2}{Z_1} \right)^\alpha \quad (3.13)$$

where U_2 is the wind speed at height Z_2 , and U_1 is the wind speed at height Z_1 . Z_2 is the computed height and Z_1 is the reference height. α is the power law exponent. The power law exponent is a function of the local climatology, topography, surface roughness, environmental conditions, meteorological lapse rate, and weather stability which is related to the wind profile logarithmically [5]. Studies have shown that the power law exponent is 0.14 or 1/7 for most sites. The wind data from NOAA was put into MATLAB, and the wind data for the corresponding height of 50 meters was calculated. The average wind speed at the NOAA station was $4.38(m/s)$ and the average speed at the corresponding height of 50 meter was $5.83(m/s)$.

The computed wind data was then analyzed and a probability density graph of the wind speed was created in MATLAB. Figure 3.15 shows a probability density graph.

The probability density graph gives a more accurate calculation of the power output. This is because the equation for power is:

$$\text{Power}(W) = SA * AD * E * 0.5 * V^3 \quad (3.14)$$

Where SA is the swept area of the turbine blade, AD is the air density, and E is the efficiency of the turbine. $(0.5 * V^3)$ is Velocity participating in a calculation of Kinetic Energy to produce the mass of air on the turbine [1]. Since velocity is cubed in this equation, doubling the wind speed would increase the power output by eight. This is why a probability density graph is better than just a yearly average. Also if the radius of the turbine is doubled the power output would increase by four.

Since the turbine will be exposed the elements of the Newport Bridge, a marine grade wind turbine was necessary for this application. The wind turbine that was chosen was the Sunforce 44444 12-Volt 400 Watt Wind Generator. The radius of the turbine is .56 meters. Thus giving a swept area of approximately $.98 m^2$. The maximum efficiency of any wind turbine can only be 59.3 % due to the Betz limit but this particular wind turbine is closer

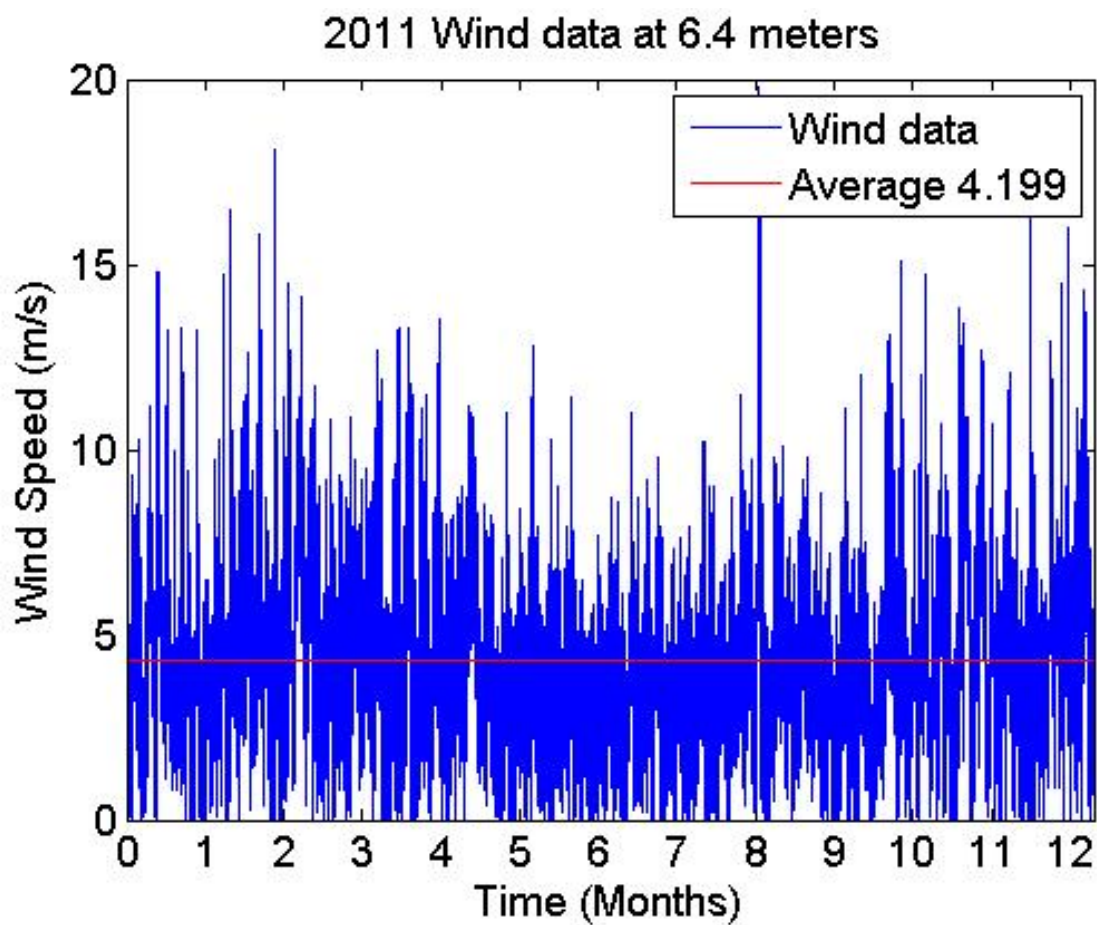


Figure 3.13: 2012 NOAA Wind Data at 6.4 meters

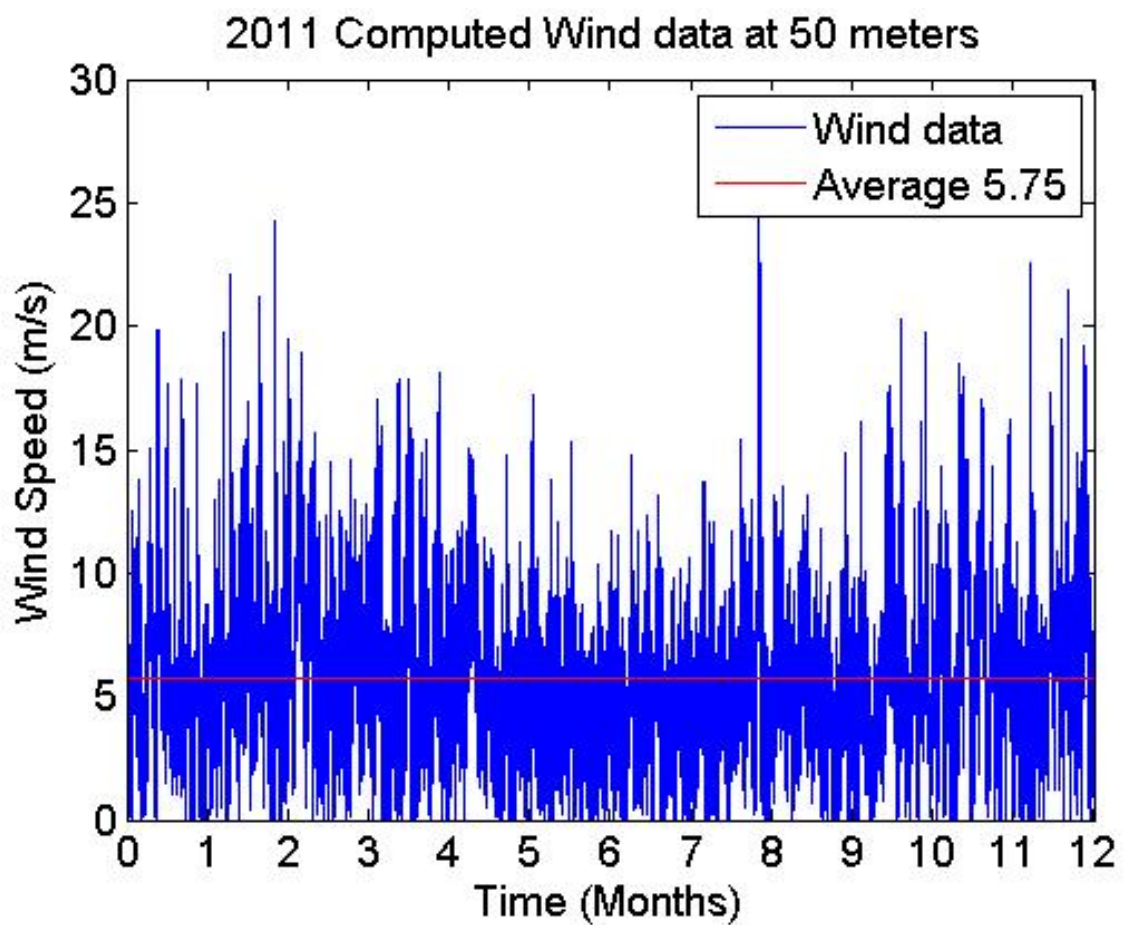


Figure 3.14: *Computed 2012 NOAA Wind Data at 50 meters*

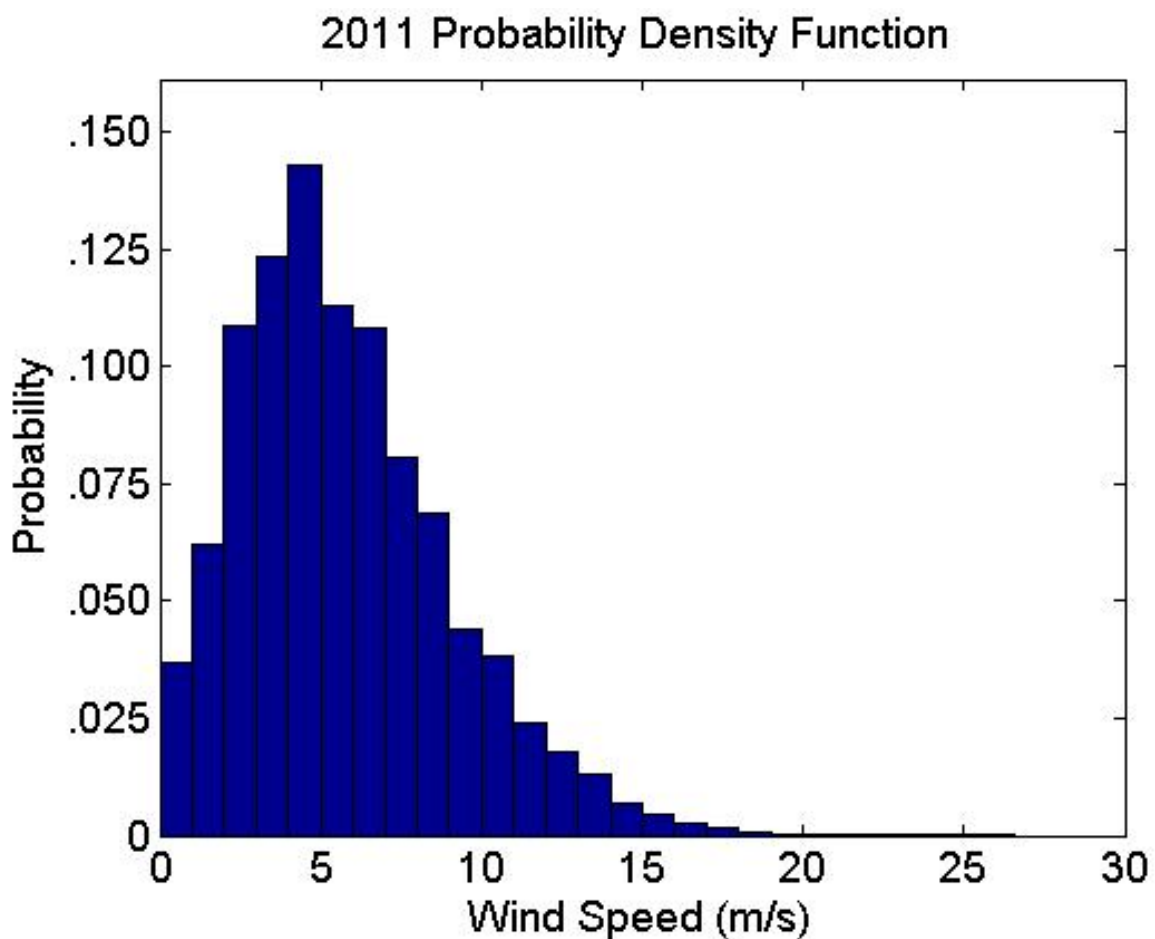


Figure 3.15: *Probability Density Graph of Computed Data*

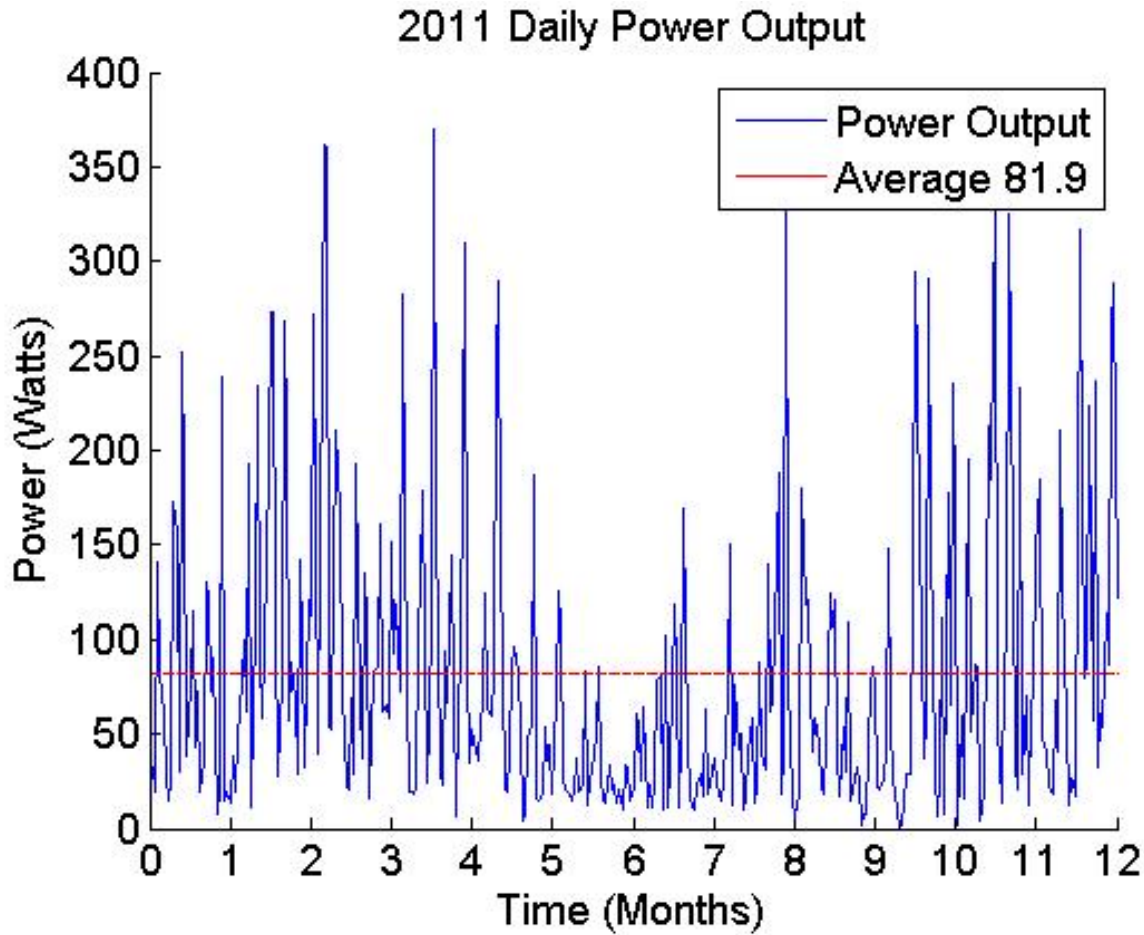


Figure 3.16: *Hourly watt output*

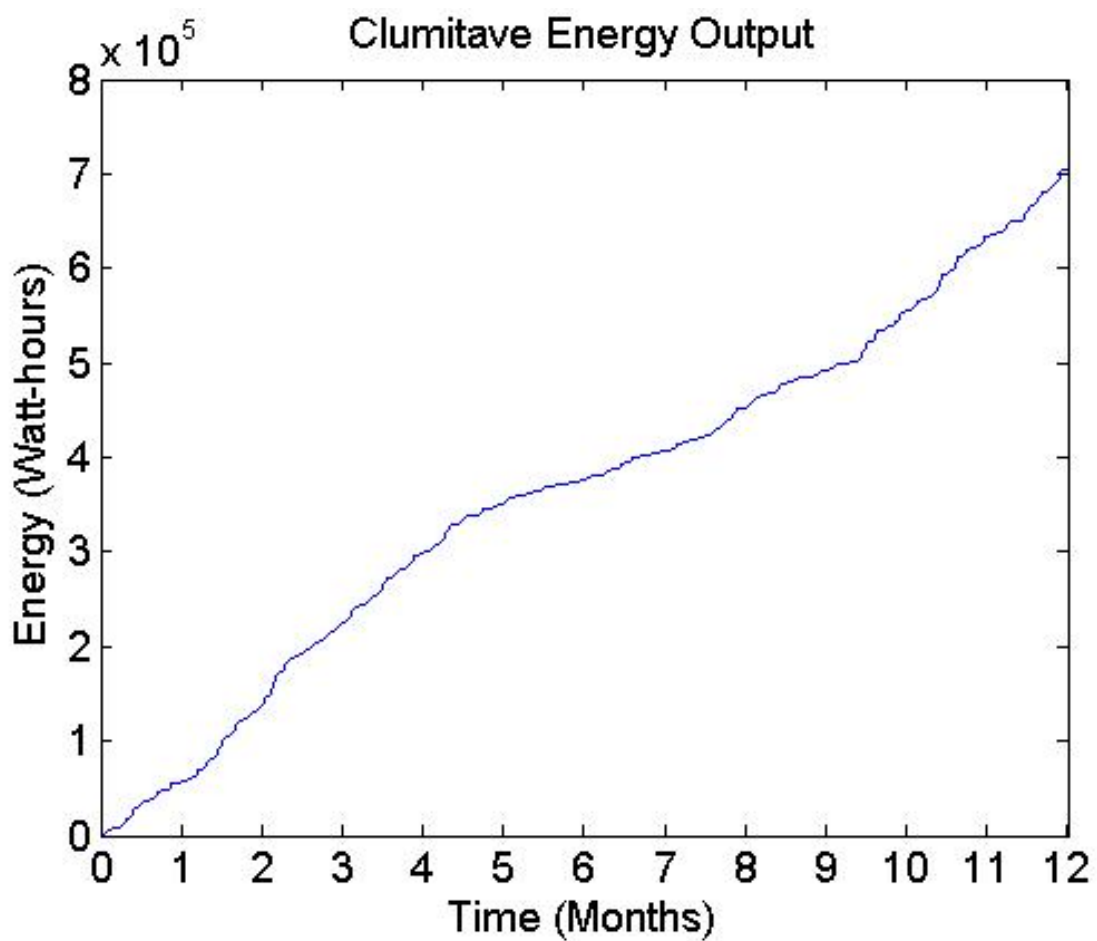
to 40%. [22].

With the power equation, turbine efficiency, and the probability density graph, an approximation can be made about the power output from the NOAA data. The hourly output can be plotted and the cumulative annual output can be calculated shown in Figure 3.16 and Figure 3.17 respectfully. For this turbine at this location the total output power was calculated to be around 700,000 watt-hours.

From the NOAA data and the wind turbine, we can determine the longest time there will be no output from the turbine. This is because the cut-in speed for this turbine is 3.2 meters per second. This will help to determine the battery size.

Year	2007	2008	2009	2010	2011	2012	2013
Hours	175	263	219	243	103	664	110
Days	7.3	10.9	9.1	10.1	4.3	27.6	4.5

Table 3.6: *Time without power production*

Figure 3.17: *Cumulative power*

3.8 Battery Selection

The factors that were important in selection of a battery for energy storage were the size and specific battery chemistry. Each battery chemistry such as lead acid, nickel metal hydride or lithium ion, have certain advantages depending on the application. Most energy scavenging systems use lead acid as they allow for trickle charging. Lead acid batteries however are larger and bulkier than others such as lithium batteries. For that reason, the battery chemistry proposed for this project was lithium polymer. Other properties to take into account when selecting a battery are the energy density as well as the number of recharge cycles one can get out of the battery. Figure 3.13 is an illustration of mass and volume energy densities specific to the various battery chemistries. It is clear that lead acid and lithium polymer reside on opposite ends of the plot. Lithium polymer batteries are exceptionally useful in applications that have space limitations such as remote operated vehicles. For this project, all of the hardware must fit inside of a case for weather proofing, making "LiPo" a reasonable selection for rechargeable battery. Another advantage to using lithium polymer is that they can be made into any shape or size. Using the power budget listed above, which highlights the power consumption relative to each piece of the package, a battery was selected. To be conservative, the power budget was doubled, making the package a 7 watt system. It was determined that in a worst case scenario, the rechargeable battery must be capable of powering the package for a minimum of 3 days. After researching various capacities of batteries, two 12 AmpHour Lithium Ion batteries were purchased. The purchase of lithium ion over lithium polymer was due to misunderstanding, however testing was still carried out in order to generate discharge curves. In the future progress of this project, the design of a charge controller capable of accepting both solar and wind as well as being able to manage the charge of lithium polymer batteries must be implemented. In order to use battery chemistries such as lithium polymer/ion coupled with such a high power wind turbine, a charge controller is paramount.

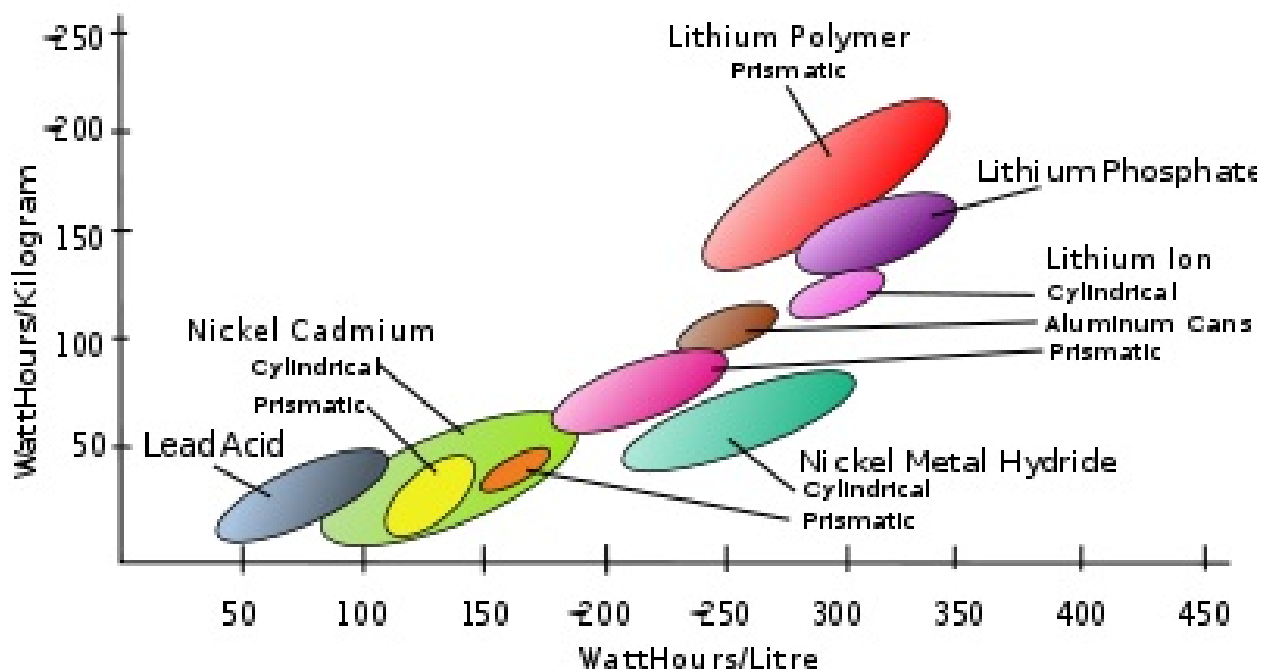


Figure 3.18: *Mass and Volume Energy Densities for Various Battery Chemistries*

Chapter 4

Data Collection

4.1 Phase One Data Collection

4.1.1 6g Tri-Axial Accelerometer Data

Vibration data for the L beam were collected with a microphone, piezoelectric strip, 3g accelerometer to computer, and 6g accelerometer from the sensor package. The only results discussed in this section are those collected from the 6g accelerometer, other results can be viewed in *Appendix ()*

Vibration frequencies of the angle beam were captured by mounting the 6g accelerometer to the beam and striking the beam. The 3 x 3 aluminum angle beam of 3/16 thickness was placed open end down with right angle pointing upward during striking. Configurations varied for supports, strike locations, and accelerometer placement locations.

The accelerometer was used to gather vibration data at four different locations. These were at a distance of $L/2$, $L/3$, $L/4$ and $L/5$ from the angle support, where L is 240 (the length of the supported section of beam).

For each accelerometer position, the beam was struck at distance $L/8$, $L/10$ and $L/16$ from the angle support. During the tests using the accelerometers, the beam was struck gently as to minimize or prevent clipping by exceeding accelerometer range of measurement.

4.2 Phase Two Data Collection

4.2.1 6g Tri-Axial Accelerometer Data

The MMA7361LC accelerometer was deployed in the computer room on the north side of the east tower, 40 feet from the top of the tower. The package collected four 60 second samples, all at 100 Hz. The package was mounted such that x is vertical, y aligned with the length of the bridge, and z is the lateral axis

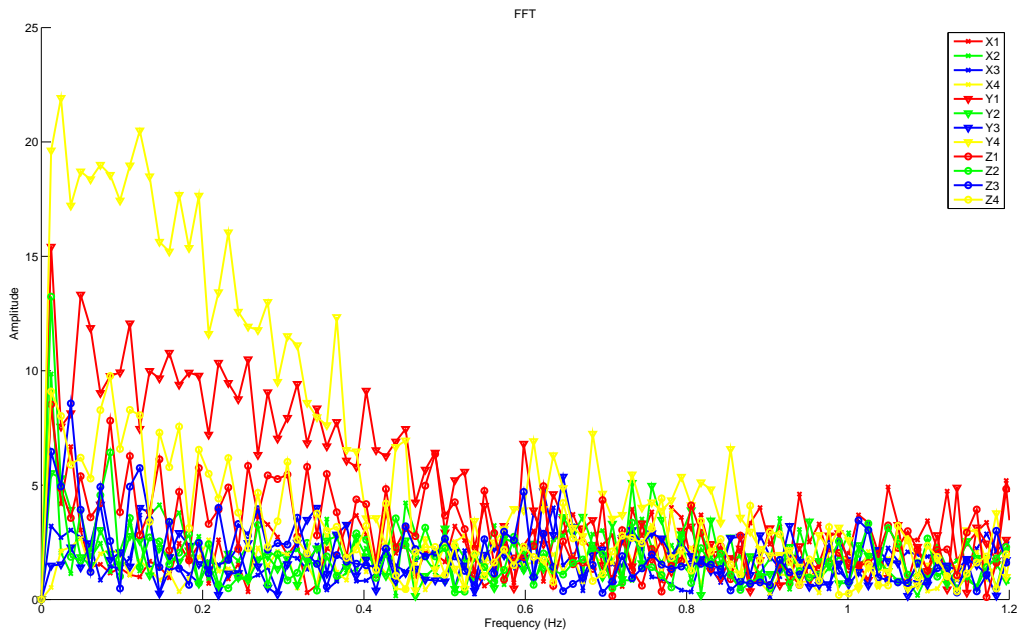


Figure 4.1: *FFT of 6g data*

The Fourier transform of each axis of each sample was taken to identify resonant frequencies . The first and fourth data set show a broadband frequency below 0.4 Hz in the Y axis, seen in figure 4.1.

Peak accelerations did not exceed 0.1 m/s^2 . Using the accelerometers 1.5 g setting would be more appropriate for this application, yielding a higher resolution.

4.2.2 Cell Phone Accelerometer

An HTC smartphone was used to collect data at various locations throughout the bridge. The Bosch bma150 3-axis accelerometer within the smartphone switches between the 2, 4, or 8 g setting. Figure 4.2 shows how each channel compares to another in a different location. The three time series are independent of each other and range from 90 to 273 seconds in duration.

The greatest accelerations are observed in the sample taken at a quarter of the length of the main span. At mid span there is a noticeable amount of acceleration but it decays to a small value around 80 seconds. The data set taken in the computer room is barely noticeable in comparison to the other two locations.

The data was low pass filtered with a Chebychev Type-II filter with a 5 Hz cutoff. It will not distort the frequencies we are expecting on the order of 1 Hz or less. Using a peak picking technique, the average frequency of the dominate vibration is 16 Hz. These points were observed in the x and y, lateral channels at midspan.

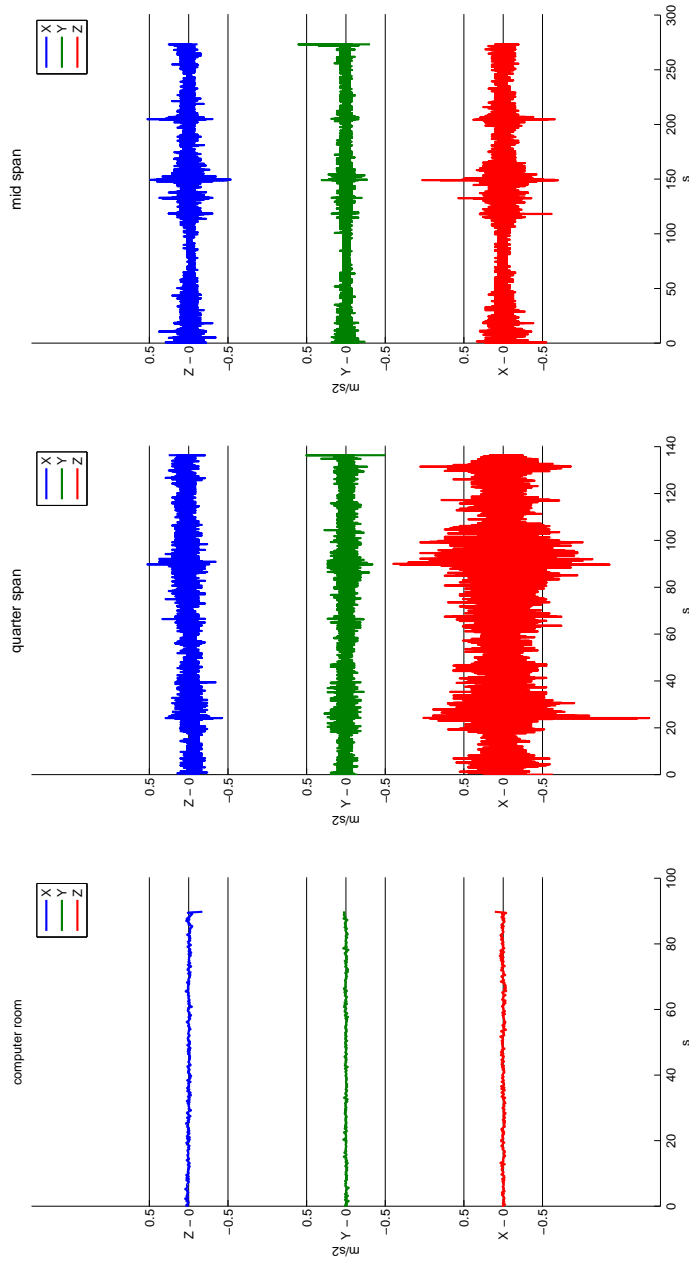


Figure 4.2: Location comparison

4.2.3 Battery Discharge

The 12 volt 12 amp hour lithium ion batteries were tested to determine how long our system would last running only on battery power. The specifications from Appendix C show the discharge rates, voltage cutoff, and how capacity varies over charge cycles.

First a Sylvania 3157 automotive light bulb was tested. The light bulb is rated for 26.88 watts. The voltage was recorded as the light bulb discharged the battery. The battery started off at 13.21 volts and discharged for 10:19:39 where it cut out at 9 volts. The light bulb draws more current than the projected package and it was decided to switch to a higher resistance load.

A pair of $100\ \Omega$ resistors were connected in parallel to achieve a measured resistance of $49.65\ \Omega$. At 12 volts the resistor will dissipate 2.88 watts of power, identical to the predicted power consumption of the package. The battery started at 13.2 volts and discharged for 20:22:12 where it cut out at 9 volts.

Figure 4.3 shows the comparison of the two loads. The shapes of the curves are identical. Decreasing the load resulted in

Current monitoring will be required to produce more accurate power curves.

4.2.4 Solar Panels

One 5 watt solar panel was attached to a 12 volt lead acid battery for testing. The current was monitored for three days, figure 4.4. On clear sunny days the panel created 0.33 amps at 12 volts. Cloud cover can cause the power to drop very rapidly.

4.2.5 Wind Turbine

The 400 watt Sunforce wind turbine was mounted atop the Fish building, URI bay campus. The ground elevation is 60 feet above the North American Datum of 1983. The location has high ground to the west as well as an adjacent building. Although this is less than ideal, it will be nearly impossible to mount the package in a location where the bridge will not block wind from one or many directions. A 60 watt light bulb was used as a load for the system.

The turbine is very responsive to changes in wind direction and is susceptible to becoming unstable during gusts. For this reason the voltage from the turbine can be seen dramatically spiking during times of the day, figure 4.5. On 02 May 2014, starting at 08:24:32 PM the turbine went for over 16 hours with zero energy produced.

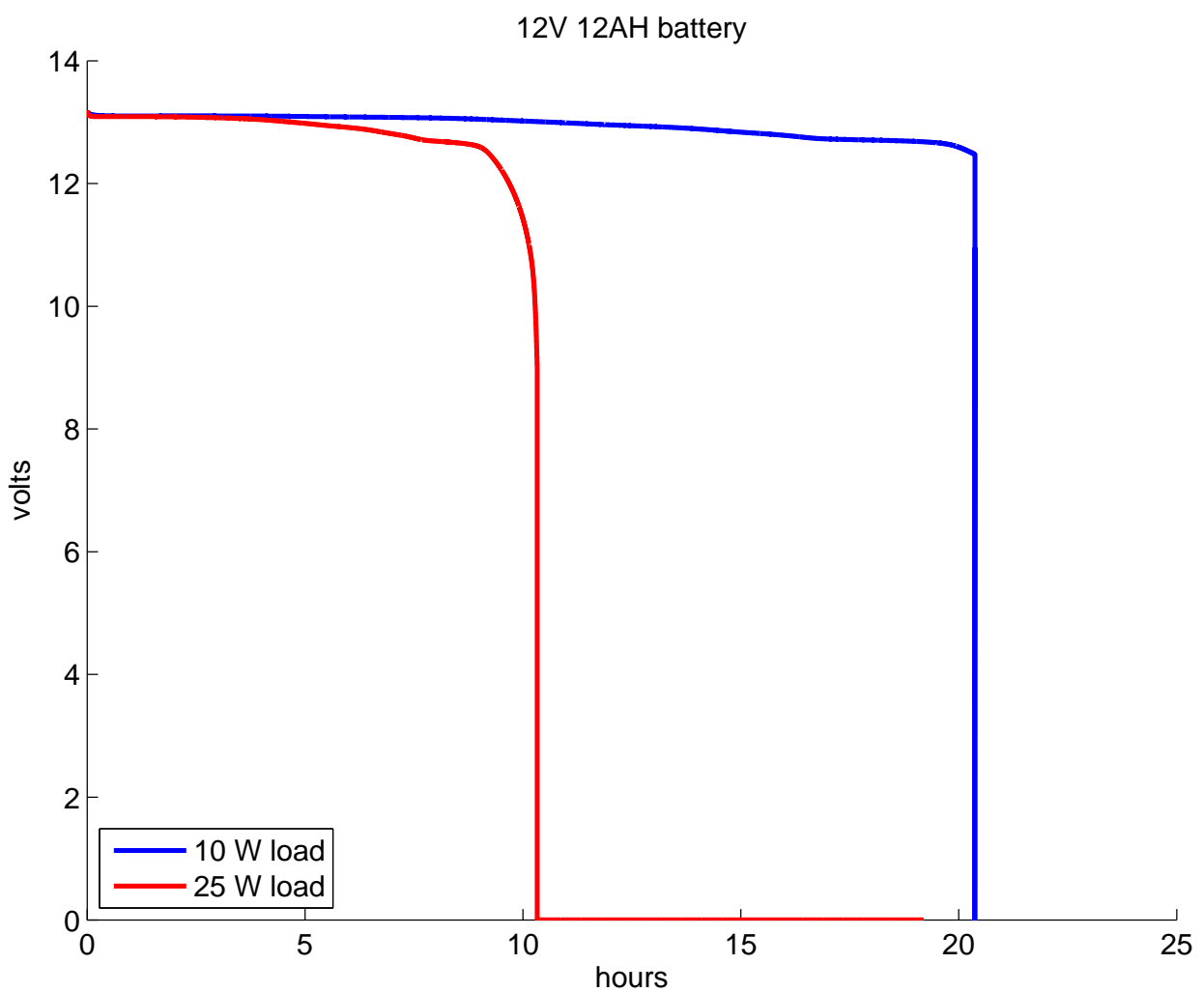


Figure 4.3: *Discharge of batteries with 2 loads*

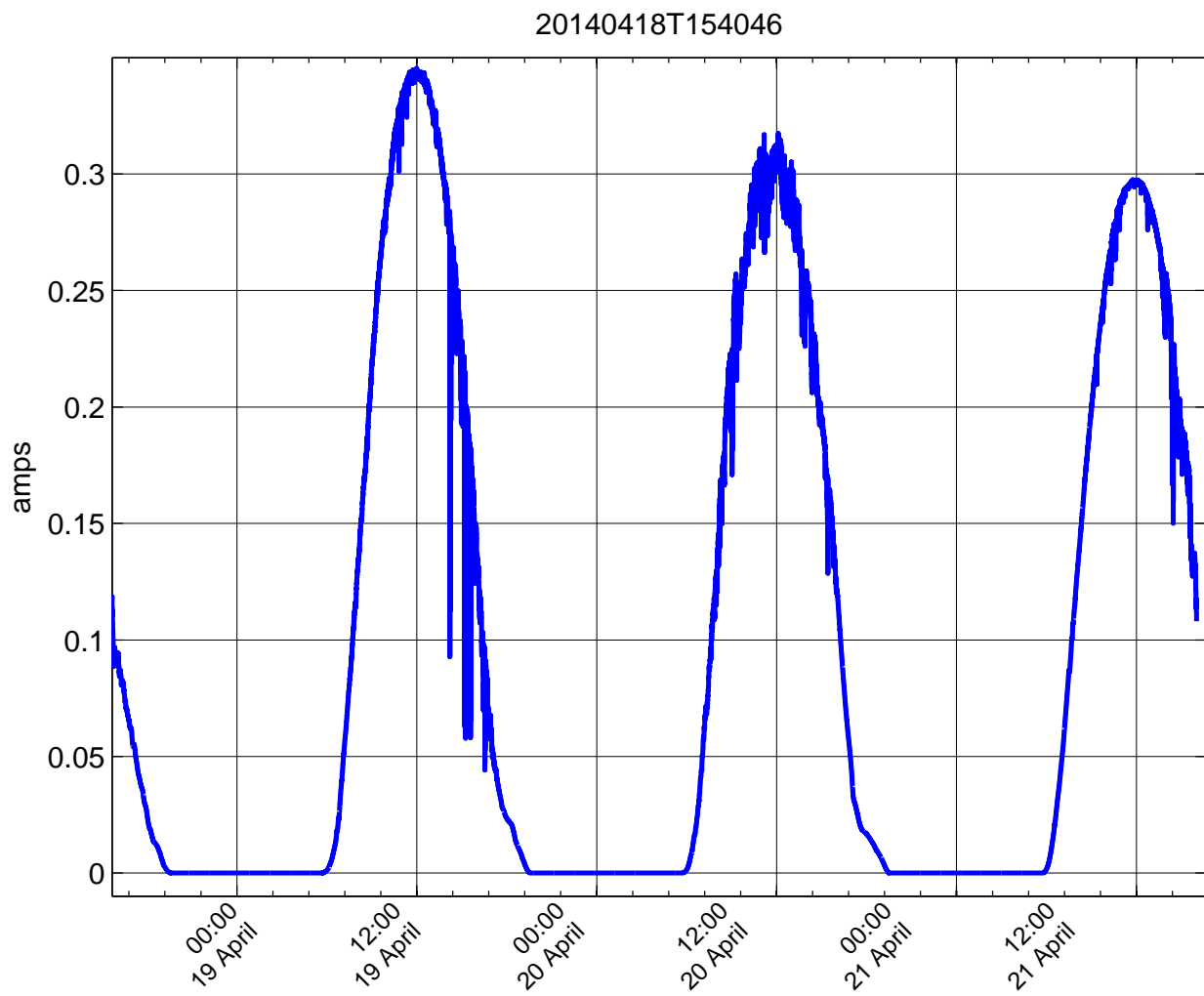


Figure 4.4: *Current output of 5W solar panel*

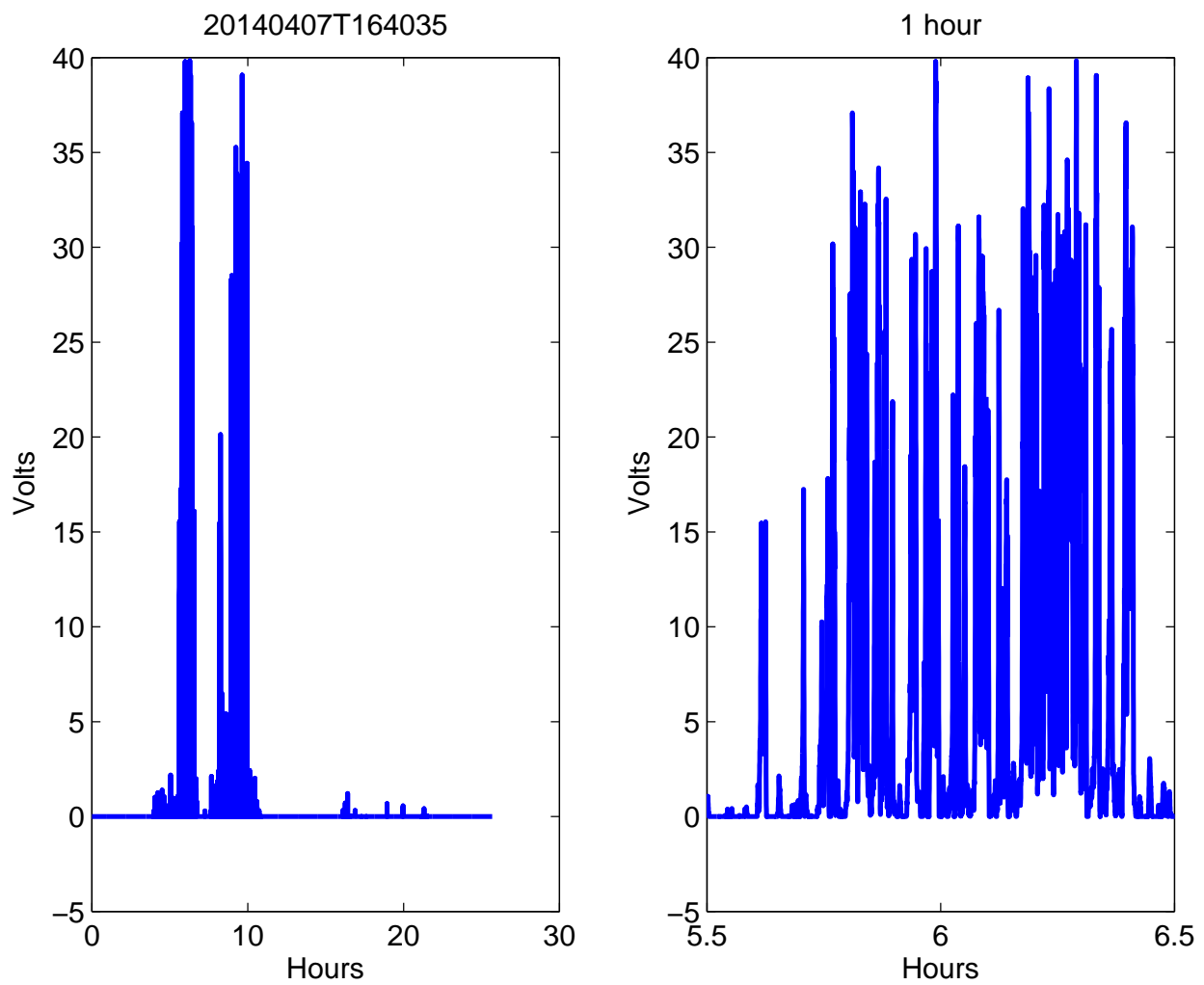


Figure 4.5: *Voltage output from turbine*

Chapter 5

Data Analysis

5.1 Phase One Data Analysis

5.1.1 Comparison of Preliminary Abaqus Model and Preliminary Data

The results of the best experimental data for the 6g accelerometer on the angle beam are shown in Table 5.1.

A direct comparison between the experimental values and the frequencies may be found in Table 5.2. As the experimental data and the analytical values are very similar the 6g accelerometer can be considered to be taking viable, accurate data. The first test was done using a piezoelectric strip to detect vibration. The second series of tests was done with a 3g accelerometer (anything above acceleration of 3g is clipped). The third series was done with a 6g accelerometer.

Mode	Analytical Values	Values for the generalized profile	Values for the Input profile	Experimental
1	3.1 Hz	3.1 Hz	3.1 Hz	3.2 Hz
2	12.4 Hz	12.5 Hz	12.4 Hz	12.5 Hz
3	27.9 Hz	27.8 Hz	27.8 Hz	27.6 Hz
4	49.6 Hz	48.8 Hz	48.6 Hz	48.4 Hz
5	77.5 Hz	74.5 Hz		78.5 Hz

Table 5.1: *Comparison between analytical, model and experimental results*

Mode	Analytical Frequencies [Hz]	Experimental Frequencies [Hz]	Percent Difference
1	3.1	3.2	3.1
2	12.4	12.5	0.80
3	27.9	27.6	1.1
4	49.6	48.4	2.5
5	77.5	78.5	1.3

Table 5.2: *Comparison between analytical and experimental results*

Mode	Journal Article Frequencies [Hz]	Abaqus Model Frequencies [Hz]	Percent Difference
1	0.16	0.135	15.62%
2	0.42	0.151	64.04%
3	0.52	0.161	69.03%
4	0.64	0.224	65.00%
5	0.71	0.259	62.51%

Table 5.3: *First five modes comparison for Abaqus and Journal Article*

5.2 Phase Two Data Analysis

5.2.1 Comparison of Developed Abaqus Model with Literature

In verifying the results of the model produced in Abaqus experimental data taken on the Claiborn Pell Bridge that were published in the Journal of the Structural Division. Upon completion in 1969 a study involving seven seismometers estimated the first 20 modes, 11 normal modal response shapes, and 20 critical damping locations. Traffic, wind, and other environmental factors loading was measured by seismometers. The direct power spectral density by way of the Ambient Vibrations Survey method was found of each recorded motion, estimates of the natural frequencies were produced. An Ambient Vibration Survey (ASV) was performed on the bridge on August 20-22, 1969. During experimentation, approximately 8,000 vehicles passed over the bridge each day and winds were moderate. Seven seismometers were arranged in five different orientations to properly capture the modal shapes. 20 natural frequencies, 11 normal mode shapes, and 20 critical damping estimates are presented. The First 20 modes of vibration ranged from 0.155-0.993 Hz, modal shapes for the first 5 symmetric vertical modes can be seen in ??

In table 5.3 the first five modal frequencies produced by the Abaqus model and that indicated by the Journal article. The fatigue that has occurred to the bridge since 1969 will account for some of the discrepancies between the frequencies as the bridge will now vibrate differently. The maximum relative difference is **PLACEHOLDER**, which shows that the frequencies calculated by Abaqus compare well with the measured and analyzed values. The main dynamic response properties of the Claiborn Pell Bridge are included in the FEM, which concur with the journal article. It is efficient to study the modal properties of the bridge using the FEM.

As the frequencies are comparable, modal shape concurrence can be looked at. The following is the modal response of the bridge as indicated by Abaqus in 5.1.

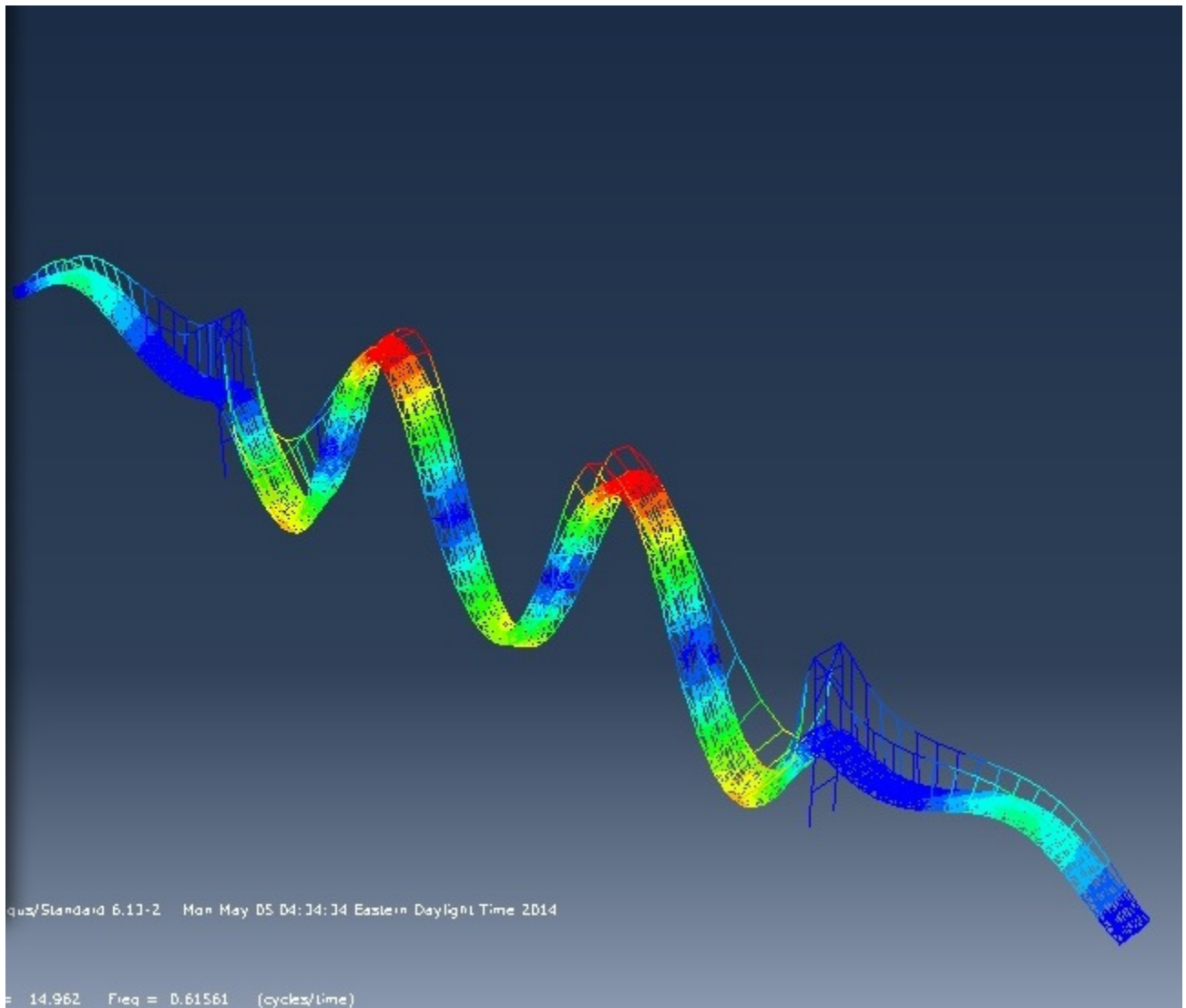


Figure 5.1: *Modal Response of Abaqus Model*

Chapter 6

Future Development

6.1 Instrumentation

6.1.1 Integration of Strain Gauge

Integration of Strain Gauge

Figure 6.1 is one of the 3-element rosette strain gauges with pre-soldered ribbon leads. Purchased from omega engineering with model number SGD-6/120RYT23. These strain gauges were necessary after realizing the difficulty of soldering leads to the original set of strain gauges. The pre-soldered ribbon leads on the second set of strain gauges also proved to be unsuccessful during experimentation. This was because the leads would not stay secured to the attaching clips while tests were being run. Even with the persistent attempts to get the strain gauges connected and working correctly, the data received was still very inaccurate. One possible contributing factor to this may have been the lack of precision when applying the strain gauge to the exact location on the beam. However, one definite factor that contributed to the inaccurate data from the strain gauges was the type of strain gauge that was used. A strain gauge with a different gauge factor and a higher resistance would have been more favorable. The higher the resistance of a strain gauge, the higher the sensitivity. The original sets of strain gauges had a resistance of $120\ \Omega$, but to precisely measure strain on a beam the resistance must be much higher, $350\ \Omega$ or more. The costs for a pack of 6 similar strain gauges with a resistance of $350\ \Omega$ from omega engineering is one hundred dollars. Another factor that halted the efforts to apply the strain gauge was that they required another ADC output. It is possible to make more outputs, however this also demands that the time synchronization is even more accurate. Nevertheless, higher resistant strain gauges would be better for sensor packages for future developments.

6.1.2 Wireless Transmission

The XBee Pro S3B long-range RF module was chosen for wireless communication between the sensor package and the base station. The unit was chosen due to its high range, up to 28 miles under ideal conditions, and relatively low power consumption (800mW). Unforeseen

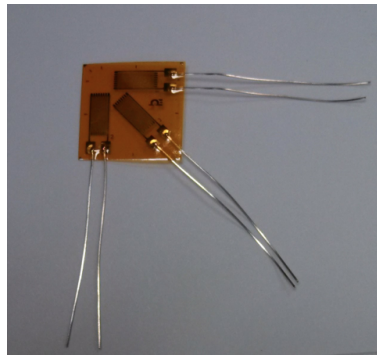


Figure 6.1: *Omega 3-Element Rosette with pre-soldered leads.*

issues were encountered when interfacing the units using the development board sold by the manufacturer, Digi International Inc. It was deemed that the task was a low priority in comparison to establishing the time synchronization of the data. Software was developed to support the RF module when the hardware issue was addressed; however this did not get completed during the project time-frame. Future development on this system is a top priority.

6.1.3 GPS Time Synchronization

Problem

The BeagleBone Black does not include a Real Time Clock (RTC). This inherently renders the internal clock unusable for reliable timing unless it can synchronize with an outside source. For this adjustment there are two options. The first is to synchronize with a network clock using NTP. This is the solution used by most laptops to supplement their bundled RTC to achieve increased accuracy. Dependant on the source, the link can provide time accuracy to tens of microseconds [11]. However, the typical accuracy falls around ten milliseconds [9]. The second option is to remove the middle man and create a time server on each server using a Global Positioning System (GPS) to set the clock. This method can result in a clock with a maximum of 100 milliseconds of error, which is unlikely [9]. For this design, the latter method was chosen based on the accuracy falling within an acceptable range and the lack of an available Wide Area Network (WAN) connection. Using individual GPS devices results in a modular system that allows for compatibility with potential mesh networks.

Synchronizing Using GPS

While the GPS atomic clock reports accuracy to 50 nanoseconds, serial interfaces are much slower with time accuracy to 1 millisecond [9]. Thus, a Pulse Per Second (PPS) signal must be used to adjust and calibrate the time. A PPS signal is a high accuracy oscillator used to increase inter-device connectivity accuracy [4]. With correct support, a PPS is typically accurate to 5 milliseconds [9]. This signal is used to adjust and synchronize the system time beyond the capability of serial GPS data. Therefore, several packages using the same PPS capable GPS receiver can be adjusted to have the same time to accuracy of

less than a millisecond without any inter-package communication.

Implementation

Using a Linux kernel allows for interfacing a PPS signal at a low level. The GPSD program allows for the interfacing NMEA standard GPS devices along with PPS support. On Linux systems, GPSD is capable of combining both NMEA sentences and PPS signals [9]. The BeagleBone Black receives the NMEA serial messages through a UART connection and the PPS signal through a GPIO pin. The Network Time Protocol Daemon for Linux allows for multiple input sources to increase accuracy. The NTPD program is responsible for setting the time on standard Linux operating systems. GPSD has the ability to broadcast the PPS and GPS time data on a local socket to make it available for third party clients. Specifically, NTPD can be set to register the sockets published by GPSD as sources. NTPD can then use the GPS data to set the system clock with accuracy below a millisecond. When multiple packages have this same setup, their clocks will be synchronized to within a millisecond. For this application, that accuracy is acceptable. Once the system clock is set, the software follows the design outlined in the Software Design section.

6.1.4 Package Assembly

Fabrication of Printed Circuit Board

The printed circuit board (PCB) described in Section 3.5.3 was not sent out to be fabricated and "stuffed". This was because of an incomplete board layout. Although all of the component footprints were created for the board, not all traces were laid. Since a board was not fabricated, it should be noted that some additions to the board would make it complete.

The following items should be added to the next revision of the PCB:

- XBee Pro S3B Wireless Receiver
- Surface-Mount Passive Components
- Breakout Headers
- Indicator LEDs

The XBee Pro S3B Wireless Receiver (or equivalent) needs to be added to the board in order to transmit data to the base station. The wireless module was not integrated into the initial design of the PCB due to inability to interface with the unit. As mentioned in 6.1.2, work needs to be focused on functionality of the wireless data transmission system.

For the initial design of the PCB, standard through-hole passive components were used for the basic circuits; resistors, capacitors, *etc.* This was done so that it would be possible to acid-etch a prototype PCB in-house prior to sending the design to a board house. This proved to not be feasible due to the footprints of the MMA7361 accelerometer and ADS1113 ADCs being surface mount components; LGA14 and MSOP-10 packages respectfully. For this reason it is no longer constituted to use large, through-hole components.

The BeagleBone Black has 92 user-accessible pins that may be used in future applications/development of the sensor board. For this reason, it is proposed that two 2x23 header

rows be connected to the header rows that the BeagleBone Black will attach to on the PCB to allow access to all pins. The same could also be done for the XBee Pro S3B and Trimble Copernicus II GPS Receiver for testing and debugging purposes.

In order to smooth the efforts of debugging, it is suggested that indicator LEDs utilized in great numbers; such that the user/developer may know which systems are receiving power, transmitting data, or in a fault state just by looking at the row of LEDs. The power budget has allocations for additional components to be added to the system. Typical surface-mount LEDs can range from 3mW to 15mW.

Package Enclosure

6.2 Package Enclosure

When the components are tested and fully operational in laboratory conditions, they will need to be packaged into the casing. The following characteristics need to be considered when determining which case is best suited for this application:

- Quality
- Size/Orientation
- Heat Dissipation
- Cost
- External Connectors

When the package is mounted onto the Newport Bridge, it will be exposed to harsh weather conditions: wind, precipitation, extreme temperatures, etc. Therefore, it is essential to utilize a case that can withstand these conditions. O-rings are necessary to prevent water from leaking into the case through the seal of the lid. This water can easily damage the electrical components within the package. The case will also have to be able to withstand possible extreme temperatures. If the case cannot withstand the possible cold temperatures it will be exposed to without cracking, water can leak into the package and destroy the equipment. High temperatures can cause the case to melt/deform which may possibly affect the retrieved data.

It will be important to choose a case that not only large enough that can house all of the equipment but also fits the equipment in a manner that it can be neatly organized and arranged. This allows for a quicker and more efficient package assembly. This also allows for a quicker examination of the set-up in case an error occurs. To account for this, the orientation of the case is important. For example, a top-loading bucket (such as the Pelican 1430 seen below) would not be practical because it would be very difficult to access the components once the package is assembled and mounted.

Electrical devices are only operational within a specific temperature range where if the maximum or minimum temperatures are exceeded, the component may not fully function or even fail completely. To determine if the SHM system will fail due to extreme temperatures,

the temperature inside the case must be calculated. The enclosed volume has two major sources of temperature flux: the external temperature and the work done by the system. The first step will be to calculate the heat transferred from the electrical components using the equation:

$$q(eq) = P(eq) * K_1 * K_2 \quad (6.1)$$

where $q(eq)$ is the heat transferred from electrical equipment in Watts (W), $P(eq)$ is the electrical power consumption (W), K_1 is the load coefficient, and K_2 is the running time coefficient. This value will then be inserted into the 1-D heat transfer equation:

$$q = k * A * \frac{\Delta T}{dx} \quad (6.2)$$

where q is the heat due to the electrical components, k is the thermal conductivity of the material, A is the area of which heat is being transferred through, ΔT is the change in temperature, and dx is the thickness of material. This equation will need to be computed for the heat transfer through each of the casing walls, as well as the corners of the case, then averaged using the equation:

$$q_t = \sqrt{(q_x)^2 + (q_y)^2 + (q_z)^2 + (q_c)^2}$$

where q_c is the heat transfer through the corners of the case. The resulting value will then be used with the maximum expected temperatures based on temperature history data, such as that provided by NOAA, to determine the maximum temperature at which the system will still operate. If the resulting temperature is higher than the lowest maximum operating temperature out of all the components, the system may fail, and that case may not be the best option. That same principal can be applied to when the system is not generating any heat with respect to the minimum expected external temperature and highest minimum operational temperature of the components. Ideally, once the package is fully modeled, the heat transfer equation can be more thoroughly and accurately calculated by accounting for the spatial orientation between the components and the interior walls of the case. However, if the components are mounted in place via foam cutouts, the heat dissipation between the components and the foam must first be calculated, and then the heat transfer between the foam and the interior walls will then be calculated.

External Connectors Several external connectors will need to be installed on the case walls for the full functionality of the SHM system. These ports need to be waterproof with tight seals to prevent water from entering the case or external connections. The waterproof connections will require secure mating mechanisms, such as locking and screwing mechanisms shown in Figure 6.2, to ensure that the male ends will not become unplugged thus allowing water to enter the connection and damage it. Each connector will also require a bulkhead cap to cover and protect against water damage if the connector is not in use. These external connections are going to be implemented for a variety of sub-systems within the SHM package: energy scavenging devices, BeagleBone Black, strain gauge, GPS, and XBee.



Figure 6.2: *Example Mating Mechanisms*

Power connectors will be used to connect the wind turbine and solar panels to the package. These connectors must be rated for a high enough current to match the power source. For example, since the wind turbine is rated up to 27A, the power connector should have a current rating that is similar enough that there will not be damage done to the port due to the excess current. Each power connection will have a female port installed on the side of the case and a corresponding male jack will need to be installed at the end of the power input. If multiple solar panels are utilized, either the power inputs need to be put into parallel in one wire to input all the energy through one connection or a connector needs to be installed for as many panels are used.

A USB 2.0A port will be installed to access the BBB without having to open the package via a flash drive. This type of USB port was chosen to match the same type of connection specified from the BBB data sheet. The connector gender of this port needs to be female to plug a USB chord to access the BBB, such as the one seen in Figure 6.3.



Figure 6.3: *USB 2.0A External Connector (LTWUA-20AMFM-SL7A) from Ampehnol LTW*

There are a few different types of connectors that can be used to attach the leads of the strain gauge to the package. Unlike the rest of the connections, the strain gauge leads do not require a certain type of connection terminal. One option is to attach the leads to either a category 5 (CAT 5) or CAT5e shielded Ethernet cable and install an external connection for such a cable as seen in Figure 6.4. Category type cables are designed for high signal integrity to achieve performance standards set by organizations [8]. This type of cable will

ensure that the signals are relayed to the ADC reliably. A shielded cable is desired to ensure that the sensitive signal being sent from the strain gauge to the ADC does not get disturbed by noise.



Figure 6.4: *Shielded Ethernet External Connector (RJ45-5EWTP-QR-PCB)* from *Video Production Inc*

An alternative method is through the use of waterproof cable glands (see Figure 6.5). The leads would be attached to a cable, preferably shielded, and fed through the gland which would then be sealed. The proper gland must be matched up to the outer diameter of the cable otherwise the gland will not be water tight. These are advantageous because not only do individual cable glands work with a range of cable thicknesses, but different gland diameter ranges can be found.

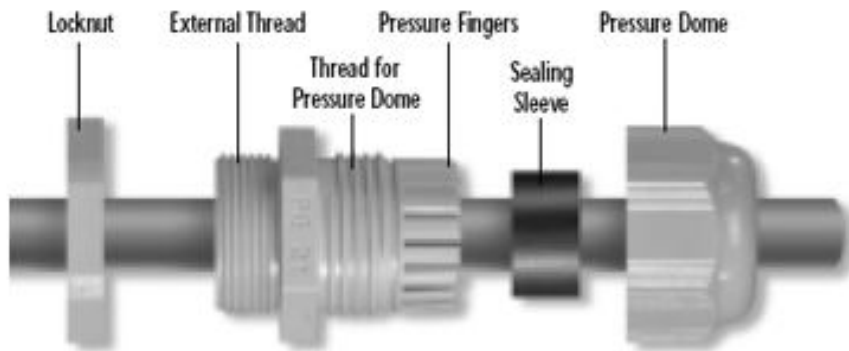


Figure 6.5: *Cable Gland (CB-GD-5000045)* from *AA Power Corp*

The GPS antenna attaches to the GPS via the use of a coaxial MCX connection. Two viable options for connecting the antenna are to implement a waterproof MCX connector or a cable gland. Implementing a waterproof MCX connector on the package may be difficult because MCX connectors are very small as evident by Figure 6.6. If one of these connectors is able to implemented, it will be essential to choose the proper impedance level of the connector. The other option is to implement a cable gland, such as the alternative option for the strain gauge above in Figure 6.5, to run a wire through the case wall between the antenna and the GPS. The antenna would then need to be fastened to the outside of the case or another substrate to prevent it from freely swinging around.

The final component that requires an external connector is the XBee. The XBee antenna attaches to the device itself via the use of an SMA connection. A waterproof coaxial connector, like the one shown in Figure 6.7, can be implemented as the external connector as well as a cable gland. Similarly to the MCX connector, the SMA connector is also small which

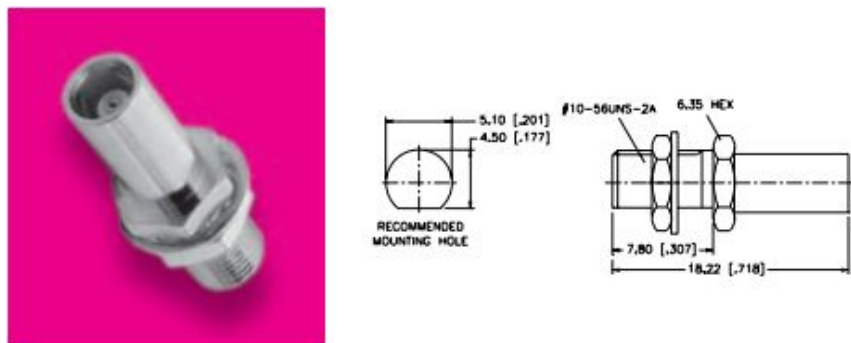


Figure 6.6: *MCX Jack-to-Jack Adapter (252171) from Aamphenol Connex with Size Reference*

may make utilizing one of these difficult. However, if a cable gland is used, the antenna may need to be mounted to the case or other substrate to prevent it from freely swinging around as is the case with the GPS.

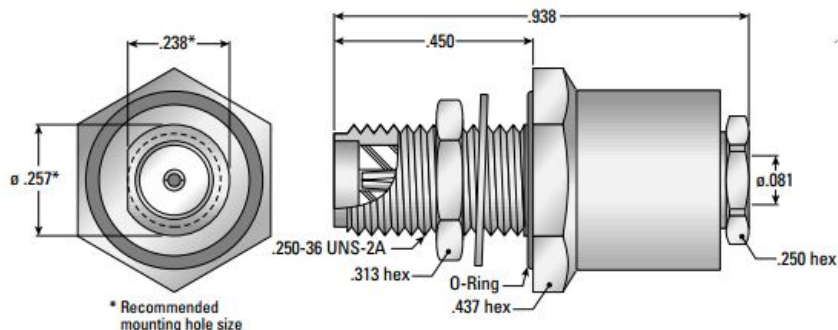


Figure 6.7: *Waterproof SMA Bulkhead Connector (9153-7553-002) from Applied Engineering Products with Size Reference*

Case Selection Attempts were made to try to obtain the actual thermal conductivity coefficients for different cases, but unfortunately proper data was never able to be retrieved due to lack of information from retailers. Since the general material of the considered cases is known, an estimation of the thermal conductivity coefficient was made because studies have been performed to determine k values for different materials. However, continued efforts to obtain this information may supply data to more accurately calculate the heat transfer through the casing walls. The thickness of each case will need to be considered for two reasons. The first reason is that the thickness of the case affects heat transfer. Thicker cases will allow for less heat transfer through the casing walls. The other is that the thickness of the casing wall affects whether or not certain external connectors can be implemented. If the case is too thick, many MCX and SMA connectors may not be able to be installed because the case may be thicker than the connector is long. When comparing costs, it should be later noted of any accessories, whether they are necessary or convenient, that can and will be purchased. For example, the Ultra-case 613 by UW Kinetics charges another \$6.99 for the required O-ring to water proof an already expensive case, so this may not be the most

suitable case for this application. For a look at the a comparison of nominal characteristics of the cases that were considered, see ??.

Assembly Layout When the package is ready to be assembled, the interior layout of the components needs to be determined. A few factors will need to be considered. The first is the location of external connectors. As stated above, the thickness of the case will affect what type of connectors may need to be used. An example of this is shown in Figure 6.8 which is a potential 2-D assembly layout using a Pelican 1400 model case. If an SMA connector were to be utilized, it would need to be used on one of the shorter walls since they are thinner. However, this SMA connector is barely longer than the case is thick and would not leave enough room to physically install it. Therefore, a cable gland would need to be utilized as an external connector for a Pelican 1400 model case. It would not make sense to install the connectors through the lid either because opening the case may place too much tension on the wires causing damage.

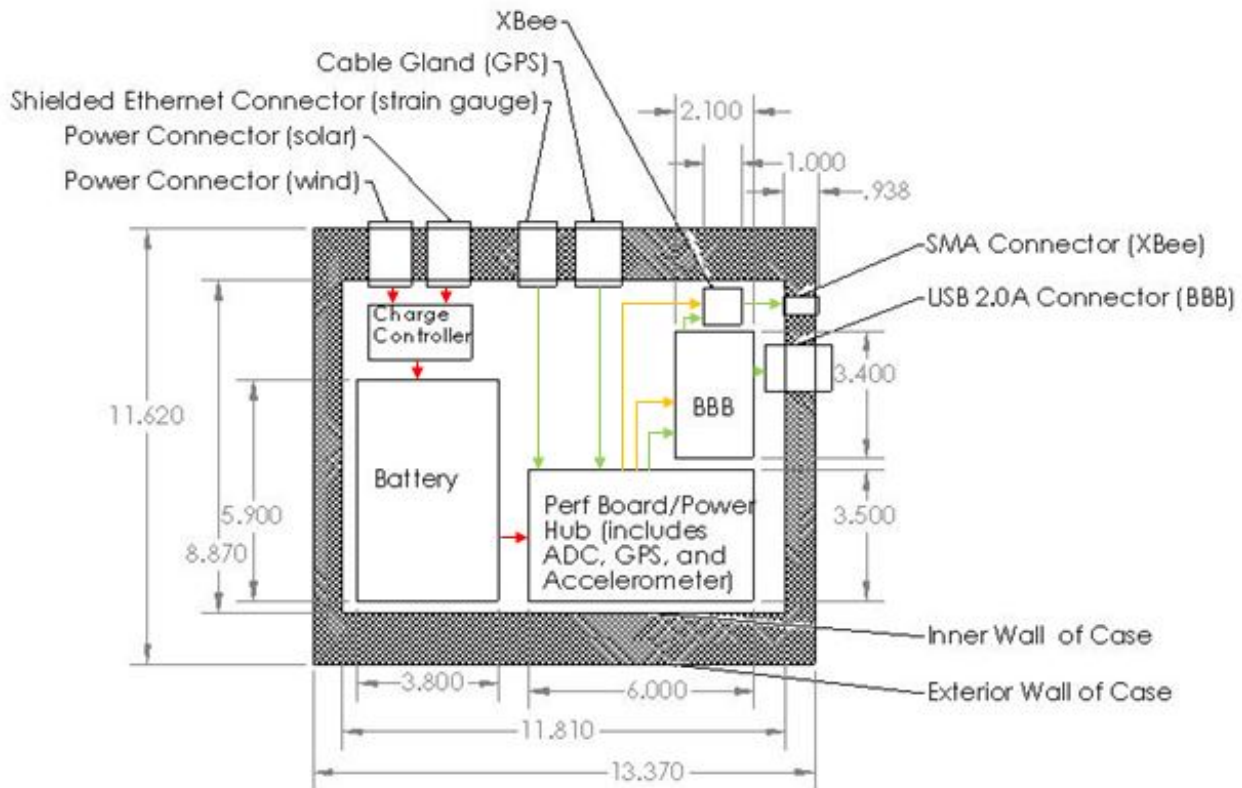


Figure 6.8: *Potential Layout of a Pelican 1400 Model Case. The red arrows depict a 12V power supply, the yellow arrows depict a 3.3V power supply, and the green arrows depict the transfer of communications.*

It will also be important to orient the breadboard in a manner that the accelerometer measures data in the intended direction as if it was mounted. Otherwise, it will need to be understood that the data measured on each axis during lab trials will not be measured along the same axes in the field and will need to be accounted for while analyzing the data.

Package Location

6.3 Package Location

Figure 6.10 is an Abaqus visualization of the Newport Bridge with the proposed location for the sensor package to be mounted. As shown in the figure, the center of the bridge is the best location for the sensor package. This is because the greatest amplitude of displacement will occur during the first mode of vibration at the middle of the bridge. Mounting the sensor package to the bridge must be done without damaging the structure in any way. The sensor package must also be capable of being moved easily. Most importantly, the package must be secured without any of its own motion so that the sensors can recognize the movement of the bridge and not the movement of the package itself.

The most economical way of securing the sensor package to the bridge is to use powerful magnets. Neodymium Magnets are strong magnets that work well in all environments and resist demagnetization. One negative aspect of magnets is that they can be prone to corrosion if a protective coating is not properly applied. There is also a concern that the magnetic field can disrupt the electronics within the case. However, these issues can be prevented if the correct precautions are taken. These magnets come in many shapes and sizes, as shown in Figure 6.9, and can be purchased with pre-fabricated holes for screws to attach the magnets to the exterior of the case. The magnets in figure 6.9 are the MMR-A-XC model of magnets from KJMagnetics.com. This magnet is hardly larger than a penny, yet it can easily be screwed into the sensor package and has a holding force of 54.14 pounds. With two of these magnets screwed into the case, the package would be secured to the bridge. If data analysis is performed to prove the wind speed on the surface of the package to be too much for this pull force, stronger magnets are available. KJMagnetics.com also has similar magnets but with different pull forces ranging from 26.8 pounds to 260 pounds. These magnets can be used for securing the solar panels and wind turbine as well.

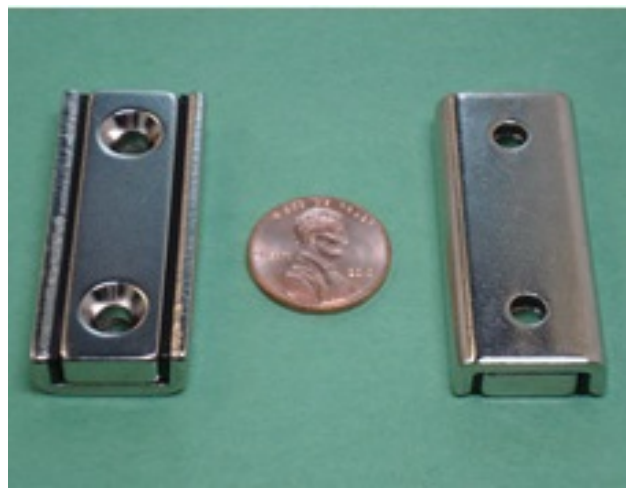


Figure 6.9: *Neodymium Mounting Magnet*

Figure 6.11 shows a practicable location for the sensor package along with the solar panels above and the wind turbine hanging just below. The sensor package should be mounted on

the outside of one of the major vertical beams at midspan of the bridge. The solar panels and wind turbine must be mounted close within a reasonable distance to keep the cable length to a minimum. The best place to mount the solar panels is on top of the upper horizontal beam on the southern side of the bridge. This will allow for the most amount of sun light and the shortest amount of cable necessary. The best place to mount the wind turbine is on the bottom of the lower horizontal beam on the southern side of the bridge. This location has plenty of wind because it is above the middle of the Narragansett Bay. By mounting the sensor package, solar panels and wind turbine below the deck on the southern side of the bridge the package will be capable of producing its own power and accurately measuring the vibrations of the bridge.

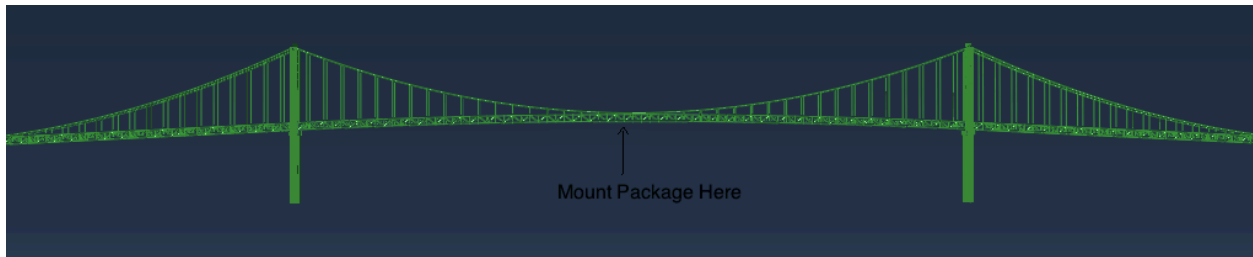


Figure 6.10: *Proposed Package Mounting Location*

6.4 FEM

6.4.1 Model Improvements

The Abaqus model produced for this project can be further developed to produce more accurate modal responses to static and dynamic loading. Any improvement to the model will replicate the bridge more closely. The longterm effect of fatigue is immeasurable and will create an unavoidable error. After measuring the current natural frequency of a bridge an original stiffness matrix can be estimated from the bridge a stiffness matrix can be estimated and inputed to Abaqus, however, evaluation the effects of fatigue on structural integrity is difficult. The current model is considered to be one cohesive piece with a uniform stiffness rather than different individual sections that are bolted or welded together. In a more precise model, as the 19,0000 element model produced for evaluating the Tsing Ma Bridge in Hong Kong, each piece of the bridge was modeled to reflect the actual material. The steel cables were molded as thousands of steel wires and the road deck was modeled as pavement [2]. As steel is primarily used for the entire structure of the Claiborne Bridge the error acquired is relatively small. Suspension bridges will deform plastically everywhere accept for the welded regions which should be modeled as rigid pieces. These joints are critical locations in the system as fatigue cracks will develop first. If the welds that are under the most stress can be identified they can be reinforced or monitored more closely [2]. Bridge scions that connect at bolts rather than welds have friction at the interface of the two sections. This friction is important when evaluating failure.

6.4.2 Dynamic Loading

In this evaluation, only static loading was evaluated as dynamic loading is outside the scope of this project. The model of the Tsing Ma Bridge was evaluated for dynamic loading as two mediums of traffic utilize this bridge. The trains and trucks that travel over the bridge require entirely separate analysis as they present the bridge with entirely different loading signatures.

The loading of a train, individual truck in both lanes, and groups of trucks with varying orientation were simulated passing over the bridge. As a single truck will not affect the net dynamic response only the local response must be examined. To minimize computation time only relevant elements were applied a tapering load for less than 2 s and then eliminated from the simulation. Groups of trucks were separated by a 3 s lag time. The variability of traffic was examined and the co-existence of the two types of loading were quantified. A stress cycle was produced for each traffic variation and compiled to identify which element would experience the most intense local stresses. The critical locations of local stress under truck loading are the utmost part of the upper chord and the bottom cross-frame between the rail tracks. Under train loading the critical locations in the deck unit are at the utmost parts of the upper chord and show more stress than the highest local stress under truck loading. Because of this it was determined that an outbound train will produce the most stress in the upper chords along the bridge longitudinal direction. This location was chosen to determine fatigue critical locations in the whole bridge [2].



Figure 6.11: *Proposed Location for Sensor Package, Wind Turbine and Solar Panels*

Chapter 7

Conclusion

Over the course of this two phase project a prototype of the sensor package was designed and partially assembled. A finite element model was produced and verified for the Claiborn Pell Bridge. Development must be done on wireless transmission of data, time-synchronization of data and energy scavenging. It is anticipated that the final sensor package will have a custom PCB designed and fabricated to localize the microprocessor, ADC, accelerometer and GPS to one board.

Bibliography

- [1] U.s. potential offshore wind energy. Technical report, ArcGIS, 2012.
- [2] Li Chan, Guo. Finite element modeling for fatigue stress analysis of large suspension bridges. *Journal of Sound and Vibration*, 261:443–464, May 2003.
- [3] Álvaro Cunha and Elsa Caetano. Experimental modal analysis of civil engineering structures. *Sound and Vibration*, 40(6):12–20, 2006.
- [4] Mills D. Pulse-per-second (pps) signal interfacing, 2010.
- [5] Zekai en. Wind velocity vertical extrapolation by extended power law. *Advances in Meteorology*, 2012.
- [6] Omega Engineeering. Omega's transactions in measurement & control. Technical report, Omega Engineeering, 2013.
- [7] Dimension Engineering. A beginners guide to accelerometers. Online.
- [8] G. Gareis. Surfaced cable filler, December 18 2003. US Patent App. 10/425,502.
- [9] Miller Gary E. and Raymond Eric S. Gpsd time service howto, 2013.
- [10] P. Horowitz and W. Hill. *The Art of Electronics*. Cambridge University Press, New York, NY, USA, 1989.
- [11] Burbank J., Kasch W., Martin J., and Mills D. Network time protocol version 4: Protocol and algorithms specification, 2010.
- [12] Shin Ae Jang. *Structural Health Monitoring for Bridge Structures Using Wireless Smart Sensors*. PhD thesis, University of Illinois at Urbana-Champaign, January 2011.
- [13] Musa Jouaneh. *Fundamentals of Mechatronics*. Global Engineering, 2013.
- [14] Walt Kester. Which adc architecture is right for your application. *Analog Dialogue*, 06(39), June 2005.
- [15] R. Kim, T. Nagayama, H. Jo, and B. F. Spencer, Jr. Preliminary study of low-cost gps receivers for time synchronization of wireless sensors, 2012.
- [16] Kistler.com. The new minnesota smart bridge. Online. via MNME.com.

- [17] MSY. Siva Prasad. Design simulation & fabrication of micromachined acceleration sensor, 2011.
- [18] Rhode Island Turnpike and Bridge Authority, 1 East Shore Road P.O. Box 437 Jamestown, RI 02835. *Pell Bridge Newport Background and History*.
- [19] SIMULIA. *Abaqus 6.13*, 6.13 edition, 2013.
- [20] R. Steigen. Modeling and analyzing a suspension bridge in like of deterioration of the main cable wires, May 2011.
- [21] Structurae. Claiborne pell bridge, July 2013.
- [22] Windpower. The betz limit. Technical report, Wind Power Program, 2008.

Appendix A

Sensor Package Schematics

A.1 LM317 Adjustable Voltage Regulators

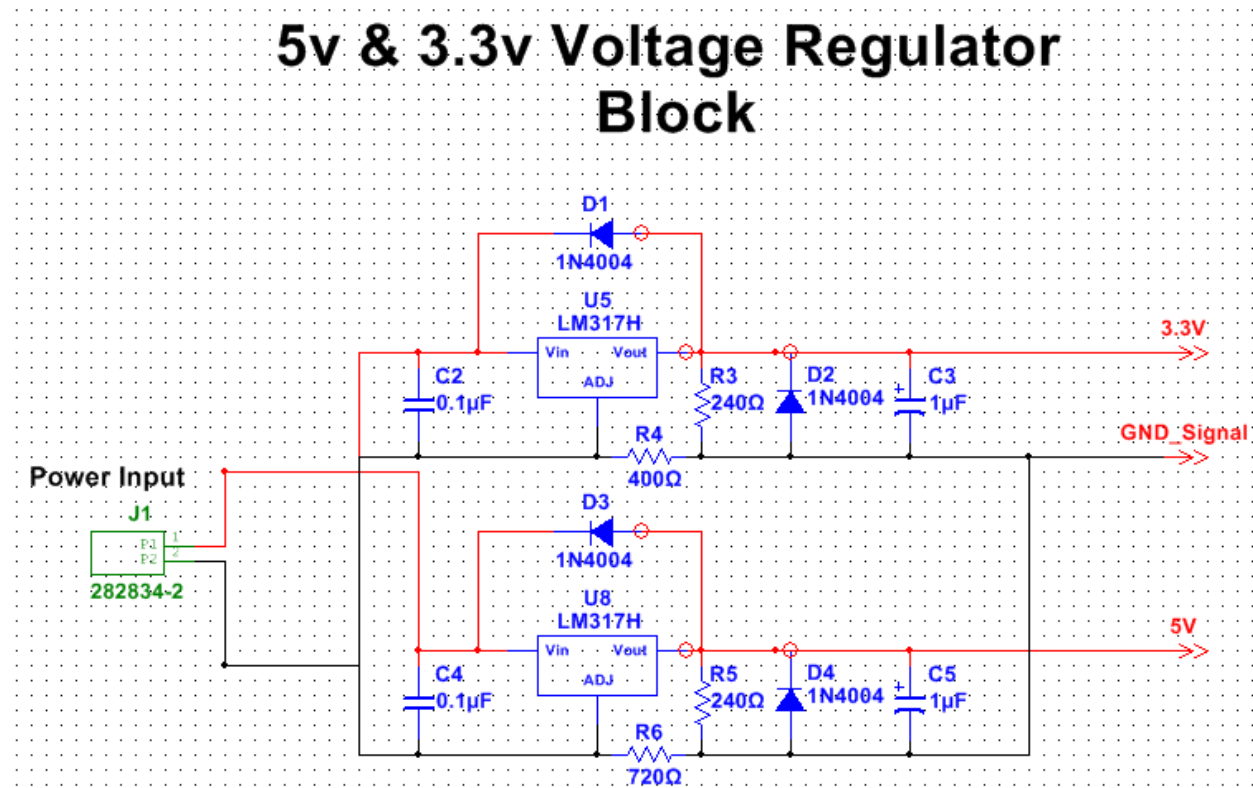


Figure A.1: *Schematic of 5V and 3.3V voltage regulator circuit*

A.2 BeagleBone Black

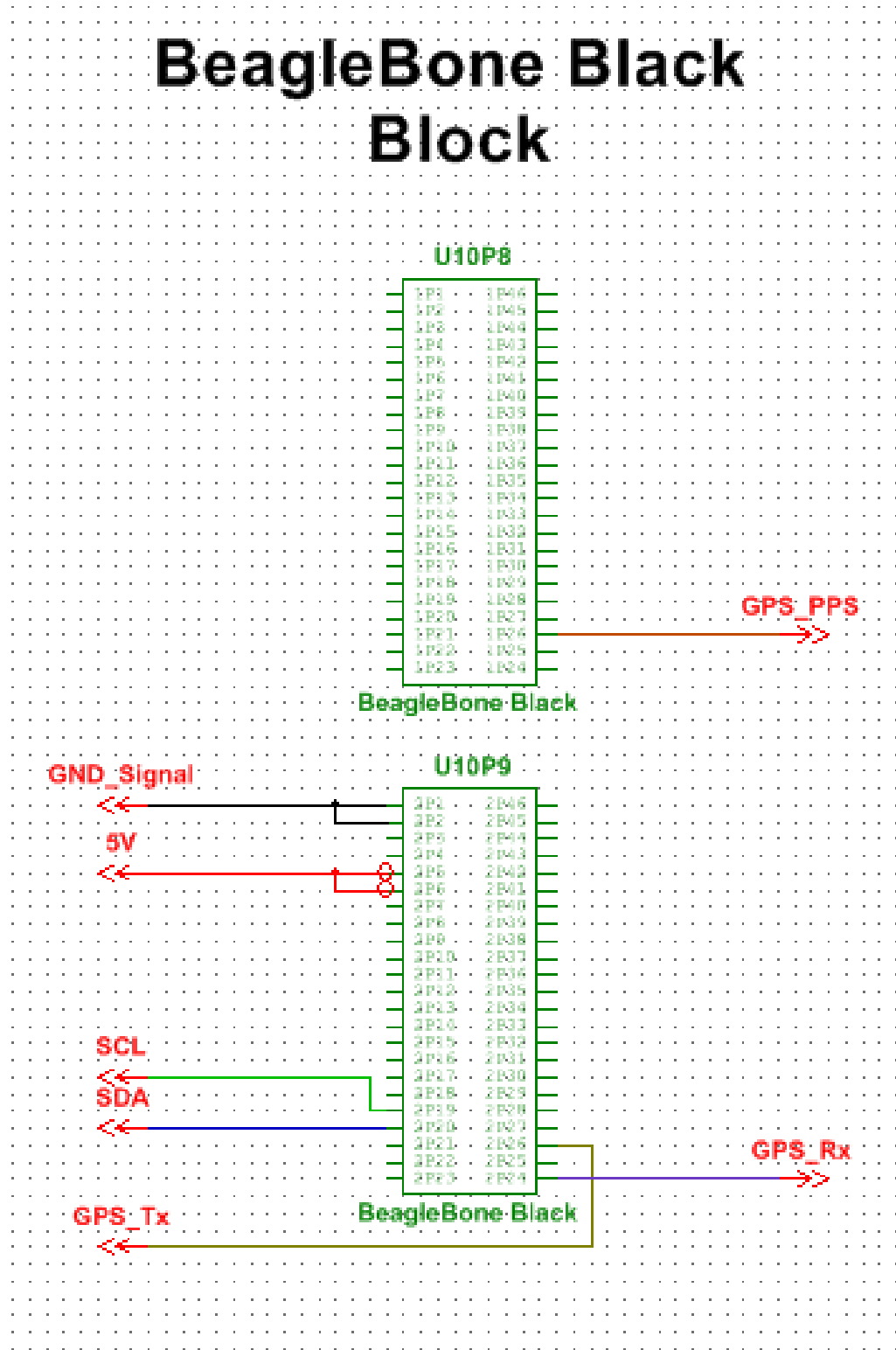


Figure A.2: Schematic of BeagleBone Black

A.3 MMA7361 Accelerometer

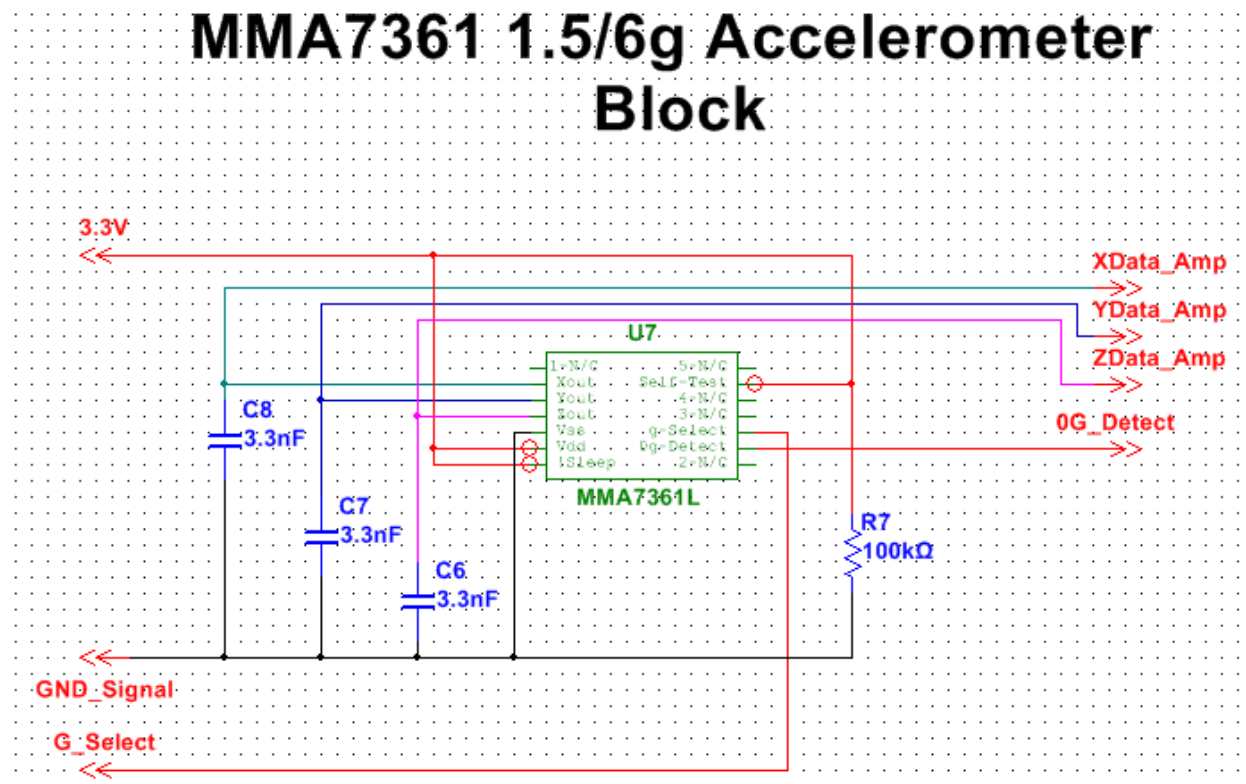


Figure A.3: Schematic of MMA7361 $\pm 1.5g$ / $\pm 6g$ Tri-Axial Accelerometer

A.4 MCP606 Op-Amp Buffer Circuit

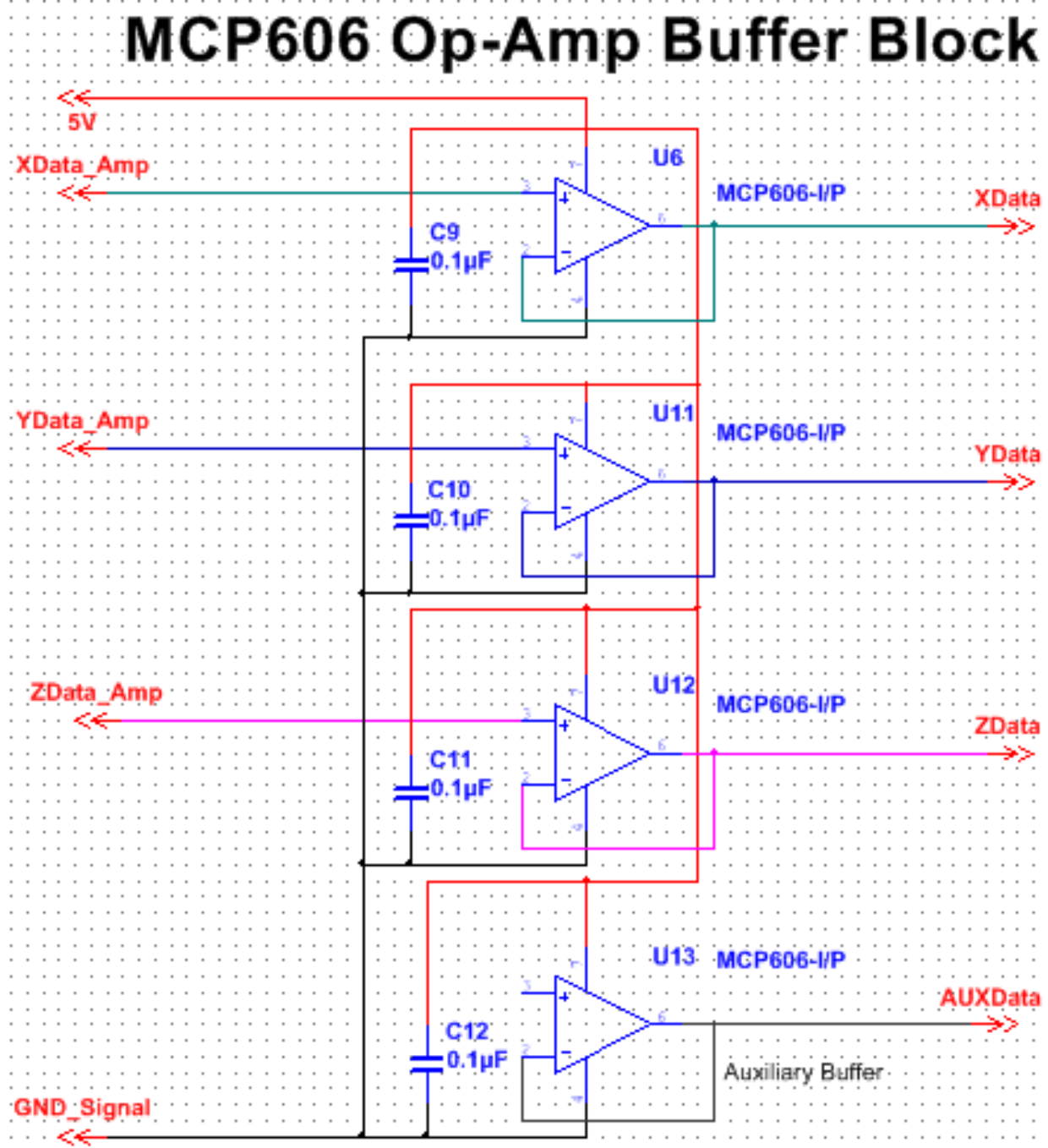


Figure A.4: Schematic of MCP606 ADC Input Buffer Circuit

A.5 ADS1113 Analog-Digital Converter

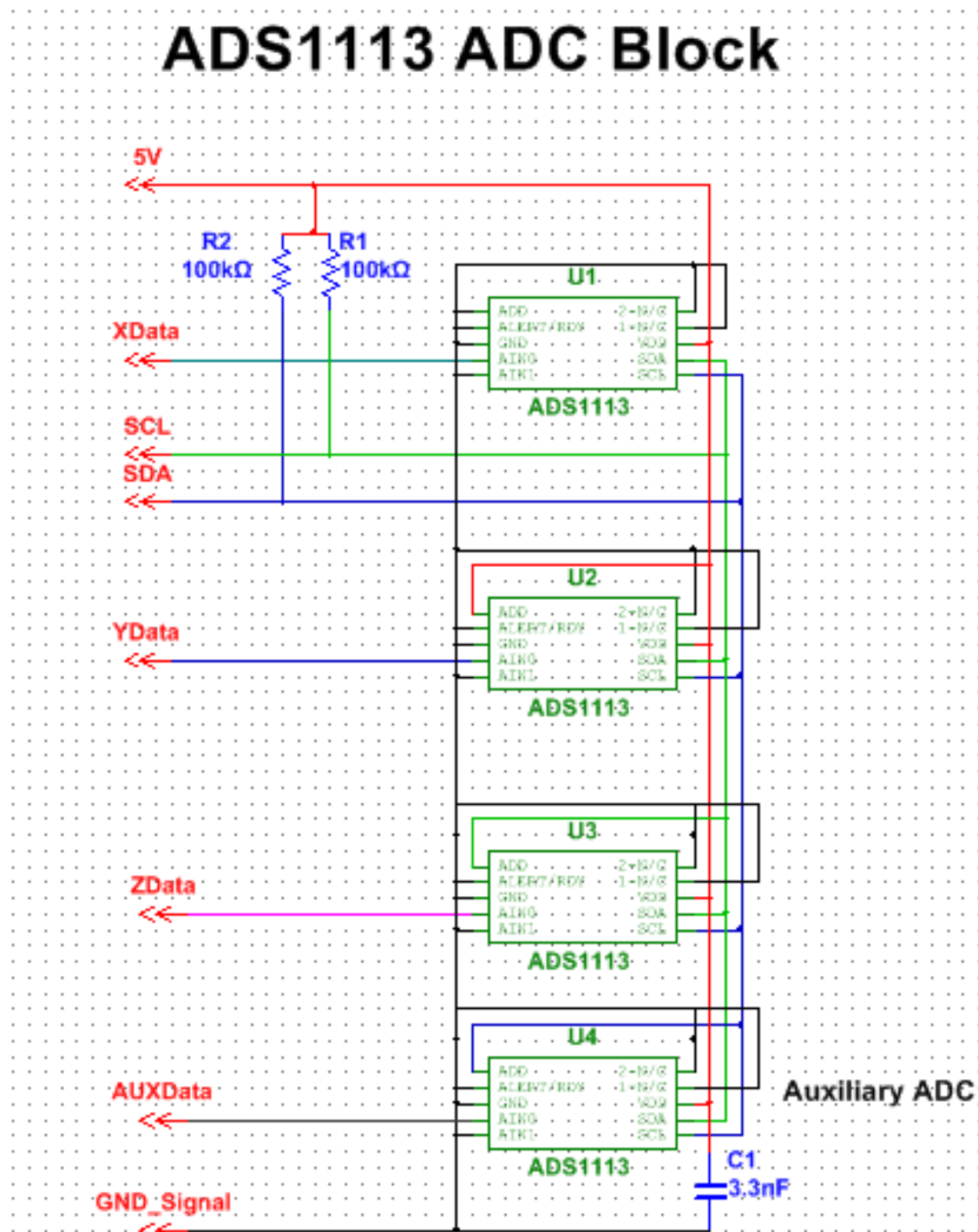


Figure A.5: *Schematic of four ADS1113 ADC units in parallel*

A.6 Trimble Copernicus II GPS Receiver

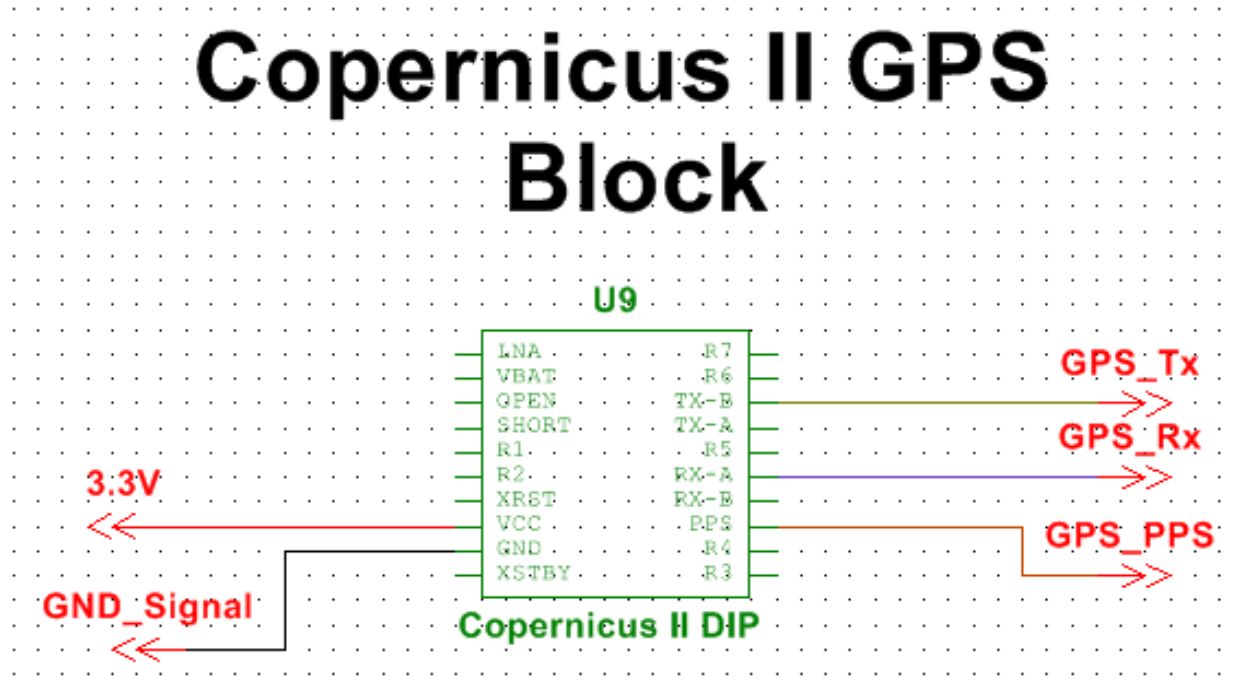


Figure A.6: *Schematic of Copernicus II GPS Receiver*

Appendix B

Enclosure Options

Company	Case Model	Enclosure Options					Cost	Thermal Conductivity Coefficient (W/m*°C)
		Length	Width	Height	Weight			
Pelican	1300	9.17	7.00	6.12	3.09	\$55.65	0.1-0.22	
	1400	11.81	8.87	5.18	3.97	\$81.58	0.1-0.22	
	1450	14.62	10.18	6	5.51	\$103.73	0.1-0.22	
	1460	18.54	9.92	10.92	8.75	\$180.59	0.1-0.22	
	PC MH 125 G	9.1	5.5	4.9	NA	NA	0.19	
Fibox	PC 2828 18 G	10.9	10.9	7.1	NA	NA	0.19	
	PC 175/150 XHG	7.1	7.1	5.9	NA	NA	0.19	
	9.4	9.4	7.4	5.5	3.3	\$38.95	0.1-0.22	
Namuk	915	13.8	9.3	6.2	4.4	\$63.95	0.1-0.22	
	UW Kinetics Ultra-case 613	13.4	8.9	5.6	4.5	\$148.99	0.2	

Table B.1: Brief summary of enclosure options considered for the sensor package

Appendix C

Battery Log

C.1 Battery Log

Filename Battery V initial load	20140421T162625 1-3 13.21 V Sylvania 3157 26.88 W 12V 2.1 A	4.24 Ω	Test on new battery 1-3 with car light
cut out V open cir	9 V 10.881 V	10:19:39	
Filename Battery V open cir	20140422T113901 1-3 10.881 V		Log of open circuit voltage from previous test
Filename Battery V initial	20140422T133734 1-3		After fully discharged battery had rested for 2 hours it was discharged again

load	Sylvania 3157 26.88 W 12V 2.1 A	4.24 Ω	
cut out V open cir	9 V 10.881 V		
Filename Battery V initial	20140422T141819 3-1 13.20 V		Part 1 of initial test on battery 3-1
load	2 x 100 resistors in parallel 49.648 observed		
Filename Battery V initial	20140423T104026 3-1 13.20 V		Part 2 of initial test on battery 3-1
load	2 x 100 Ω resistors in parallel 49.648 Ω observed		
cut out V open cir	8.962 V 10.96 V	20:22:12	